



# Determination of $\text{NO}_x$ emission rates of inland ships from onshore measurements

Kai Krause<sup>1</sup>, Folkard Wittrock<sup>1</sup>, Andreas Richter<sup>1</sup>, Dieter Busch<sup>2</sup>, Anton Bergen<sup>2</sup>, John P. Burrows<sup>1</sup>, Steffen Freitag<sup>2</sup>, and Olesia Halbherr<sup>2</sup>

<sup>1</sup>Institute of Environmental Physics, University of Bremen, Bremen, Germany

<sup>2</sup>State Agency for Nature, Environment and Consumer Protection in North Rhine-Westphalia (LANUV NRW), Recklinghausen, Germany

**Correspondence:** Kai Krause (kakrau@iup.physik.uni-bremen.de)

Received: 8 August 2022 – Discussion started: 16 August 2022

Revised: 22 February 2023 – Accepted: 7 March 2023 – Published: 3 April 2023

**Abstract.** Inland ships are an important source of  $\text{NO}_x$ , especially for cities along busy waterways. The amount and effect of such emissions depend on the traffic density and  $\text{NO}_x$  emission rates of individual vessels. Ship emission rates are typically derived using in situ land measurements in relation to  $\text{NO}_x$  emission factors (e.g. the number of pollutants emitted by ships per unit of burnt fuel). In this study, a different approach is taken, and  $\text{NO}_x$  emission rates are obtained (in  $\text{g s}^{-1}$ ). Within the EU LIFE project, CLean INland SHipping (CLINSH), a new approach to calculating the  $\text{NO}_x$  emission rates from data of in situ measurement stations has been developed and is presented in this study. Peaks (i.e. elevated concentrations) of  $\text{NO}_x$  were assigned to the corresponding source ships, using the AIS (automated identification system) signals they transmit. Each ship passage was simulated, using a Gaussian puff model, in order to derive the emission rate of the respective source ship. In total, over 32 900 ship passages have been monitored over the course of 4 years. The emission rates of  $\text{NO}_x$  were investigated with respect to ship speed, ship size, and direction of travel. Comparisons of the onshore-derived emission rates and those on board for selected CLINSH ships show good agreement. The derived emission rates are of a similar magnitude to emission factors from previous studies. Most ships comply with existing limits due to grandfathering.

The emission rates (in  $\text{g s}^{-1}$ ) can be directly used to investigate the effect of ship traffic on air quality, as the absolute emitted number of pollutants per unit of time is known. In contrast, for relative emission factors (in  $\text{g kg}^{-1}$  fuel), further knowledge about the fuel consumption of the individual

ships is needed to calculate the number of pollutants emitted per unit of time.

## 1 Introduction

In cities along busy waterways such as the Rhine, the diesel engines of inland vessels are a significant source of emissions of pollutants (i.e. oxides of nitrogen ( $\text{NO}_x = \text{NO} + \text{NO}_2$ ), carbon monoxide (CO), and aerosols). The total amount and effect of these emissions depends on the traffic density along those waterways and the emissions of the individual vessels. In order to limit the effects of these emissions on air quality, the Central Commission for the Navigation of the Rhine (CCNR) and the EU have established, during the past few decades, regulations for ship engines (The European Parliament and the European Council, 1998, 2016; CCNR, 2020). However, these regulations only apply to new engines (new ship construction or replacement of old engines). Engines on ships already in service are subject to grandfathering and do not have to comply with newer regulations. The effect of these requirements is therefore limited, as ship engines have a long service life. There is no provision for continuous monitoring of emissions from ships in service, as is the case with road vehicles, for example. To determine the emissions of ship traffic, there has been a lack of measurements of both the ship traffic and the emissions from the different types of ship engines during the real cruising operation. Consequently, a large number of assumptions had to be made in order to determine the mean emissions caused by the ships.

Shipping emissions have been typically investigated using in situ instruments, either on board or onshore (e.g. Moldanová et al., 2009; Alföldy et al., 2013; Diesch et al., 2013; Beecken et al., 2014; Pirjola et al., 2014; Beecken et al., 2015; Kattner et al., 2015; Kurtenbach et al., 2016; Kattner, 2019; Ausmeel et al., 2019; Celik et al., 2020; Walden et al., 2021). Additionally, remote sensing techniques such as differential optical absorption spectroscopy (DOAS; e.g. Berg et al., 2012; Seyler et al., 2017, 2019; Cheng et al., 2019; Krause et al., 2021) and more recently unmanned aerial vehicles (UAVs) are used to investigate ship emissions (Zhou et al., 2019, 2020). In most studies, ship emissions are investigated only for short time periods or only specific ships are investigated. Usually, emission factors in fuel (either  $\text{g kg}^{-1}$  or  $\text{g kWh}^{-1}$ ) are derived, but some studies also derive emission rates (e.g. in  $\text{kg h}^{-1}$ ). NO<sub>x</sub> emission factors (in  $\text{g kg}^{-1}$  or  $\text{g kWh}^{-1}$ ) can be derived from simultaneous NO<sub>x</sub> and CO<sub>2</sub> measurements. To convert the emission factors to emission rates, additional knowledge about the fuel consumption of the individual vessels would be needed. However, emission rates can be derived directly and are usually reported by studies using remote sensing techniques. For example, Berg et al. (2012) showed the capability of airborne DOAS measurements to derive the NO<sub>2</sub> and SO<sub>2</sub> emission rates of sea ships. But other remote sensing techniques such as lidar (Berkhout et al., 2012) or UV cameras (Prata, 2014) can also be used to derive the SO<sub>2</sub> emission rates for sea ships. In general, there is a lack of long time observations of emission factors or emission rates, especially for inland ships. The long-term impact of shipping emissions has been investigated by modelling studies (Eyring et al., 2005; Ramacher et al., 2018, 2020; Tang et al., 2020; Wang et al., 2021; Jiang et al., 2021).

Within the EU LIFE project, CLean INland SHipping (CLINSH), two methods to measure ship emissions were used. In situ instruments on board ships were deployed to measure the emissions of the engines directly at the exhaust. Measurements were carried out on 40 inland vessels which participated in the project. Absolute NO<sub>x</sub> emission rates (in  $\text{g s}^{-1}$ ) have been derived from these measurements. In addition, a method to derive absolute NO<sub>x</sub> emission rates from the onshore measurements of passing ships has been developed and is presented in this study. The retrieval concept builds on the approach presented in Krause et al. (2021), but the method has been improved, and the algorithm can now be used with data measured by any standardised in situ measurement station located in the vicinity of a river.

In total, more than 32 900 ship passages have been identified and analysed between 2017 and 2021 and provide a data set, which will be used in the future update of the inland waterway vessel emission register of the state of North Rhine-Westphalia. Generally, the NO<sub>x</sub> emission rates reflect the real sailing conditions at this part of the Rhine. The derived NO<sub>x</sub> emission rates may be used directly as input for models that describe the emission of ships and differentiate

between ship sizes and speeds over ground. Similarly, the derived NO<sub>x</sub> emission rates can be used to build a ship emission inventory for the Lower Rhine area. In contrast to more regularly reported emission factors (in  $\text{g kg}^{-1}$  or  $\text{g kWh}^{-1}$ ), the derived NO<sub>x</sub> emission rates may be used directly without further assumptions regarding the fuel consumption of the ships, as the fuel consumption is already accounted for in the NO<sub>x</sub> emission rates. At the same time, the NO<sub>x</sub> emission rates are only strictly correct for this specific part of the Rhine and cannot be easily adapted to other rivers.

## 2 Measurement sites

For the CLINSH project, the State Agency for Nature, Environment and Consumer Protection in North Rhine-Westphalia (LANUV NRW) set up continuous measurement stations in Duisburg at the Duisburg–Rhine Harbour (DURH) and in Neuss at the Neuss–Rhine Harbour (NERH), which measure the NO<sub>x</sub> concentration and meteorological parameters such as atmospheric pressure, humidity, temperature, wind speed, and wind direction close to the river Rhine.

### 2.1 Instrumentation

Instrumentation at both measurement sites along the river Rhine, Duisburg–Rhine Harbour (DURH) and Neuss–Rhine Harbour (NERH), was identical (for specifications, see Table 1). Nitrogen oxides were measured with an AC32M from ENVEA (formerly Environnement SA), 3.5 m above ground, while meteorological parameters were obtained with a weather station from LAMBRECHT meteo GmbH during the course of the campaign. The weather sensor measured wind speed ( $U$ ) with a rotary anemometer and wind direction ( $\theta$ ) with a wind vane at 10 m above ground. The time resolution for both measurement types is 0.2 Hz or 5 s.

The measurement principle to obtain NO and NO<sub>2</sub> is based on the emission of light during the chemical reaction between NO and ozone in the reaction chamber of the instrument. This reaction is called chemiluminescence and corresponds to the oxidation of a NO molecule by ozone to an excited state (NO<sub>2</sub><sup>\*</sup>; Reaction R1). During the decay to its electronic ground state, the molecule emits light in a spectrum from 600 to 1200 nm (Reaction R2), which is measured with a photomultiplier. Since each molecule emits a defined amount of light, the measured signal is proportional to the sum of the NO molecules in the air sample. The NO<sub>2</sub> concentration in the air sample is determined indirectly in a second step by converting it to NO in a hot molybdenum converter (Reaction R3) and subsequently oxidising it with ozone, as described above. This yields NO<sub>x</sub>, from which the concentration of NO<sub>2</sub> is obtained by subtracting the previously measured concentration of NO. These measurements correspond to the standard reference method specified in the DIN EN 14211. Molybdenum converters have known

**Table 1.** Specifications of the instruments used.

Measurements at DURH and NERH	Specifications
Nitrogen oxides	NO <sub>x</sub> (NO + NO <sub>2</sub> )
Instrument	AC32M
Manufacturer	ENVEA (formerly Environnement SA)
Measurement principle	Chemiluminescence
Measurement range	NO: 0–1200 µg m <sup>-3</sup> NO <sub>2</sub> : 0–500 µg m <sup>-3</sup>
Measurement accuracy	15 %
Air sampling height	3.5 m above ground level
Meteorological parameters	Wind speed ( <i>U</i> ); wind direction ( <i>θ</i> )
Instrument	EOLOS-IND static weather sensor
Manufacturer	LAMBRECHT meteo GmbH
Measurement range	<i>θ</i> : 0–360° <i>U</i> : 0.1–85 ms <sup>-1</sup>
Measurement accuracy	<i>θ</i> : ±3° <i>U</i> : ±0.5 ms <sup>-1</sup>
Measurement height	10 m above ground level

cross-sensitivities to other oxidised, atmospheric odd nitrogen species (e.g. HNO<sub>2</sub>, HNO<sub>3</sub>, and HONO), which can lead to the overestimation of the NO<sub>2</sub> and NO<sub>x</sub> levels.



Additionally, the measurement stations are equipped with AIS (automatic identification system) receivers, which deliver information on the passing ships. Under favourable wind conditions (wind blowing ship plumes towards the in situ systems), both measurement stations show strong enhancements of NO<sub>x</sub> when ships pass the measurement site, which can be clearly seen as a peak in the time series. Different views of the measurement sites are shown in Fig. 1.

## 2.2 Duisburg–Rhine Harbour (DURH)

In Duisburg, the measurement site is located on the eastern riverbank of the Rhine (51.460721° N, 6.727486° E; 28 m a.m.s.l. – above mean sea level). As the predominant wind direction has a westerly component, emissions from ships are transported towards the measurement site for the majority of the time. Consequently, a large number of pollution peaks from ships passing are identified in the measured NO<sub>x</sub> concentration time series (e.g. Fig. 2). Generally, this measurement site is well located to derive NO<sub>x</sub> emission rates from ships sailing along the Rhine because it is close to the Rhine and the entrance to the DURH basins. Conse-

quently, the measured concentration peaks can be differentiated for ships that pass the measurement site in different sailing conditions (e.g. ships that sail upstream against the river current or downstream with the river current). This measurement station was set up in October 2017 and is still active at the time of writing. In this study, measurements from 2017 until the end of 2021 are evaluated.

## 2.3 Neuss–Rhine Harbour (NERH)

In contrast to the measurement site DURH, the measurement site in Neuss is located within the Neuss harbour area on the western side of the Rhine (51.219577° N, 6.704074° E; 30 m a.m.s.l.). Buildings and vegetation block the direct line of sight from the measurement station to the Rhine. The combination of its location and the predominant southwesterly wind direction leads to only a few plumes being detected from ships that are steaming along the Rhine at this measurement site. Nevertheless, due to its location directly within the harbour, this measurement site is well suited to evaluate the emissions of slow-moving ships within the harbour area, where the influence of the river currents on engine operation are negligible. This measurement station was set up in September 2017 and dismantled at the end of 2019. Therefore, NO<sub>x</sub> emission rates could be derived for the years 2017 to 2019.

## 3 Methods

Combining the onshore in situ measurements of NO<sub>x</sub> and the received AIS signals enables the ship emission rates from passing ships, identified by AIS, to be calculated. The approach uses three consecutive steps, which are described in the following.

### 3.1 Peak identification

The first step is to identify the peaks of NO<sub>x</sub> caused by passing ships. To identify these peaks, a low-pass-filtered time series is calculated from the measured time series using a running median with a window length of 5 min. This low-pass time series describes the changes in the background concentration caused by meteorological factors and other emission sources but excludes the short-term variation caused by passing ships. The low-pass-filtered time series is then subtracted from the measured time series, resulting in a time series which is close to zero on average but still shows the sharp peaks caused by the passing ships. This time series is then analysed. If the NO<sub>x</sub> peaks exceed a defined threshold, then the peak is defined as a NO<sub>x</sub> plume most likely caused from shipping. The threshold is selected to ensure that the peaks are due to the enhancement of NO<sub>x</sub> caused by point sources, such as ships, and not noise in the measurements. In this case, the threshold was defined as 2 ppbv (parts per billion by volume). For each identified peak, the time of occur-



**Figure 1.** Views of the two different measurement sites used in this study. The upper row shows a satellite image of the DURH station and a picture of the measurement container, as seen from the Rhine. The lower row shows a picture of the measurement container in the NERH and a satellite picture of its location.

rence ( $t_{\text{peak}}$ ), the peak width, and the height of the maximum above the background concentration are determined.

### 3.2 Ship assignment

The second step is to identify the respective source of the peak. For each peak, all ships within a 5 km radius around the measurement site up to 5 min before the peak maximum were investigated. For each ship, the corresponding AIS signals within the given time frame are collected and interpolated to a 1 s time resolution. For each AIS signal position, a trajectory is calculated to assess whether the emissions caused at that specific ship position could have been transported to the measurement site by the wind. The wind speed and direction used for these trajectories are the 30 min averages of wind speed and wind direction at the measurement site. Each trajectory is calculated for the period between the time stamp of the AIS signal ( $t_{\text{AIS}}$ ) and the time of the peak maximum ( $t_{\text{peak}}$ ). It is then checked to see whether the trajectory ends within a 50 m radius of the measurement site. If only the trajectories of a single ship end close to the measurement site in the selected time window, then the source of the NO<sub>x</sub> peak is assigned to this ship. If no trajectory ends within the 50 m radius, then the peak is considered to be caused by a source other than a ship and is not analysed further. For cases where

several ships are identified as possible sources of the peak, these peaks are not analysed further because the unambiguous assignment of the source of the NO<sub>x</sub> emission to a single ship is not feasible. Once a ship has been identified as the source of the NO<sub>x</sub> peak, the relevant information (e.g. position, course, and speed) for that particular ship passage is assigned to the peak. The first assigned ship position is the position transmitted 180 s before  $t_{\text{AIS}}$ , and the last assigned position is the position 180 s after  $t_{\text{peak}}$ . The selection of these start and end points ensures that the entire NO<sub>x</sub> emission plume from a particular ship during its passage across the measurement site is recorded.

### 3.3 Calculation of emission rate

In the third step, the NO<sub>x</sub> emission rate for each peak assigned to a source ship is calculated. As the stations only measure the concentration of NO<sub>x</sub> at the measurement site and not at the stack of the ship, a model has to be applied to estimate the emission rate from the concentration enhancement found at the measurement site. The method which we have chosen is to assume that the plume of the ships can be described by a Gaussian puff model, as follows (Zenger, 1998):

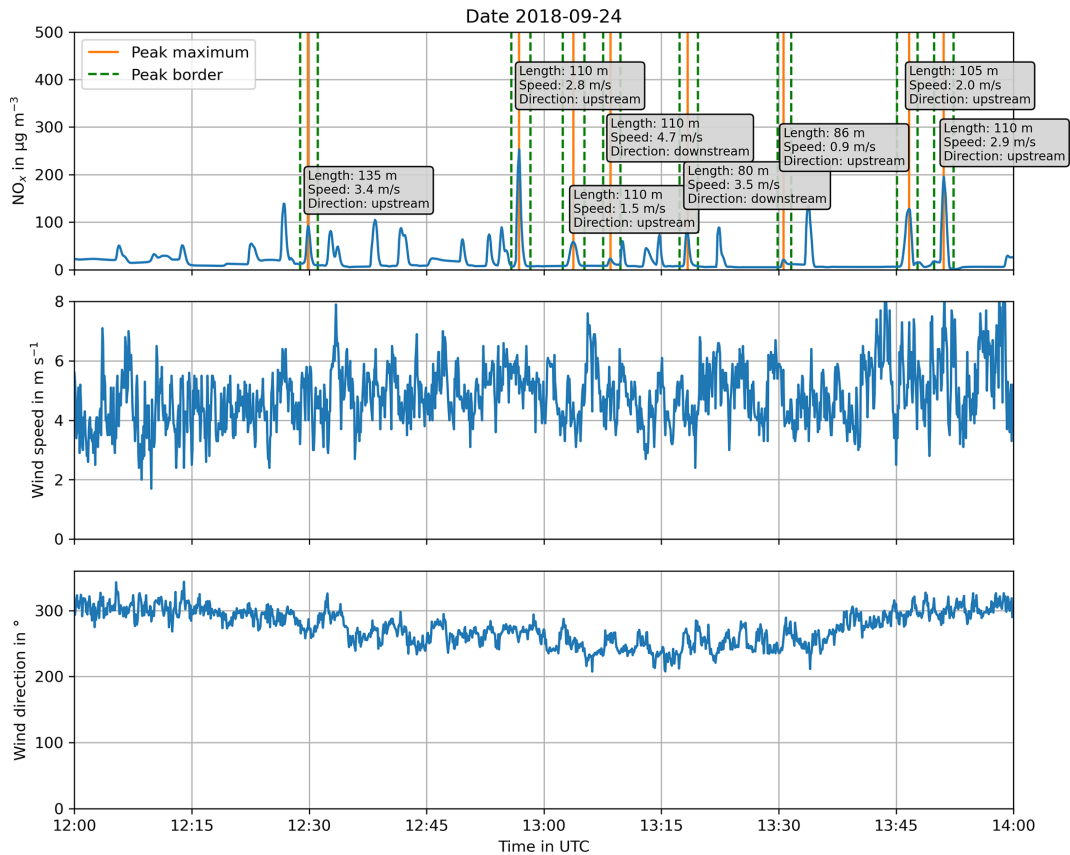


**Figure 2.** Example of the measured NO<sub>x</sub> concentration, wind speed, and wind direction at DURH (5 s time resolution). Ship peaks identified in the NO<sub>x</sub> concentration are marked with an orange line, and their borders are dashed green lines. The text box at each peak shows the ship length (in m), the speed over ground (in m s<sup>-1</sup>), and the direction of travel (upstream or downstream). Peaks without a label are most likely also caused by passing ships. In these cases, an unambiguous assignment of a source was not possible.

$$\begin{aligned}
 C(x, y, z) = & \sum_{i=1}^N \frac{Qdt}{\sigma_x \sigma_y \sigma_z (2\pi)^{1.5}} \\
 & \cdot \exp\left(\frac{-(x - U \cdot (t - dt))^2}{2\sigma_x^2}\right) \\
 & \cdot \exp\left(\frac{-y^2}{2\sigma_y^2}\right) \cdot \left[ \exp\left(\frac{-(z - H)^2}{2\sigma_z^2}\right) \right. \\
 & \left. + \exp\left(\frac{-(z + H)^2}{2\sigma_z^2}\right) \right], \tag{1}
 \end{aligned}$$

where the concentration at a point ( $C(x, y, z)$ ) is assumed to be a function of the emission rate ( $Q$ ), the dispersion due to atmospheric stability ( $\sigma_x, \sigma_y, \sigma_z$ ), the length of time of the emission ( $dt$ ) at a certain source point ( $x = 0; y = 0$ ), funnel height ( $H$ ), the total transport time ( $t$ ), and the wind speed ( $U$ ). The wind direction is taken to be along  $x$ . The funnel height is assumed to be 5 m above the mean water level, which was always assumed to be at the surface level ( $z = 0$ ).

The height of 5 m was chosen because it is assumed that the plume quickly bends down due to the wind and movement of the ship. The height was always assumed to be the same, as most inland ships share a similar distinctive form, with the funnel at the back of the ship having similar heights. The model releases a puff of pollutants at the ship's position, which is then transported by the wind for an amount of time ( $t - dt$ ) and dispersed according to the current atmospheric stability. The time ( $t$ ) is different for each ship position and is always the time of the last AIS signal of the ship passage ( $t_{\text{peak}} + 180$  s) minus the time of the respective AIS signal ( $t_{\text{AIS}}$ ). The result is a concentration field caused by the emission of pollutants at the specific ship location for a time step  $dt$ . This procedure is then repeated for all ship positions. The calculated concentration fields then describe how the plume developed during the ship passage (e.g. Fig. 3).

As the emission rate is unknown, the model is run with an arbitrary but constant emission rate ( $Q_{\text{model}}$ ). The height of the plume centre is approximated to be at the height of the funnel above water level, assuming that the plume quickly bends down due to the wind and movement of the ship. It is also assumed that this height is roughly the same for all

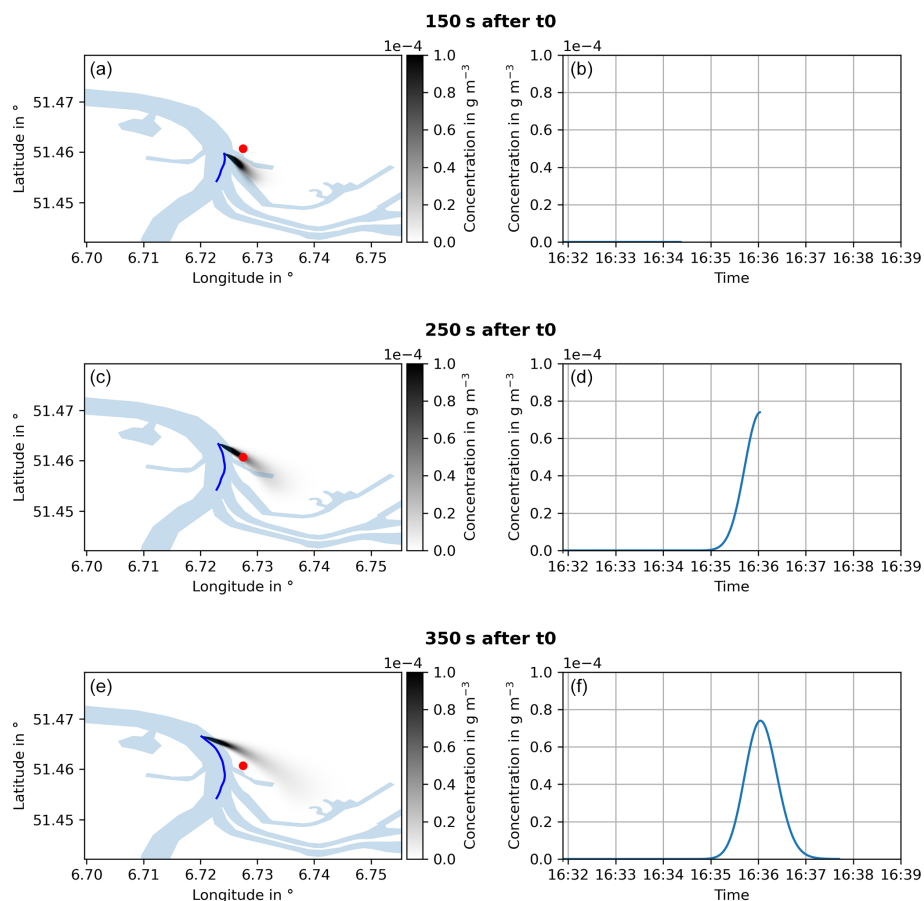


**Figure 3.** Example of a plume simulation for different time steps after the simulation start ( $t_0$ ). The upper, middle, and lower panels show the movement of the modelled ship plume 150, 250, and 350 s after the initiation of the plume. (a, c, e) A horizontal cross section of the modelled plume with 20 m height. The location of the measurement station is marked as a red dot. The blue line in panels (a), (c), and (e) shows the modelled concentration at the location of the measurement station during the model run.

ships. Dispersion parameters are chosen according to the atmospheric stability, which has been determined using the wind speed at the measurement site and incoming global radiation (DWD Climate Data Center, 2021) during the day and with cloud coverage (DWD Climate Data Center, 2022) during the night from a nearby weather station of the German Weather Service located at Düsseldorf International Airport. To derive the emission rate, the integrated measured concentration, i.e. the area under the peak ( $C_{\text{meas}}$ ), which has been corrected for the fluctuating background, is compared to the modelled concentration at the measurement site, i.e. the area under the modelled peak ( $C_{\text{model}}$ ). Assuming that the model sufficiently describes the ship's plume, the only difference between modelled concentration and measured concentration is caused by the different emission rate. Consequently, the emission rate of the ship ( $Q_{\text{meas}}$ ) is estimated by the following equation:

$$Q_{\text{meas}} = \frac{C_{\text{meas}}}{C_{\text{model}}} \cdot Q_{\text{model}}. \quad (2)$$

This approach assumes that the emission rate is constant for the whole modelled time domain. An example is shown in Fig. 4. In contrast to Krause et al. (2021), the whole ship passage is modelled, which allows the modelling of the transport and dispersion of the emitted trace gases as a function of time. Consequently, the peak area can be used to derive the respective emission rate of the ship, whereas in Krause et al. (2021), only the peak maximum was identified and compared with the modelled maximum to derive the emission rate. In comparison, using the peak area is a more reliable measure than the peak maximum because it relates the total number of pollutants arriving at the measurement site.

### 3.4 Quality control

The assumptions made in the model to estimate the NO<sub>x</sub> emission rate may not truly represent the conditions at the time of measurement. To assess the quality of the derived emission rate, Monte Carlo simulations are performed to assess whether a small change in one of the input parameters results in a large change in the derived concentration at the

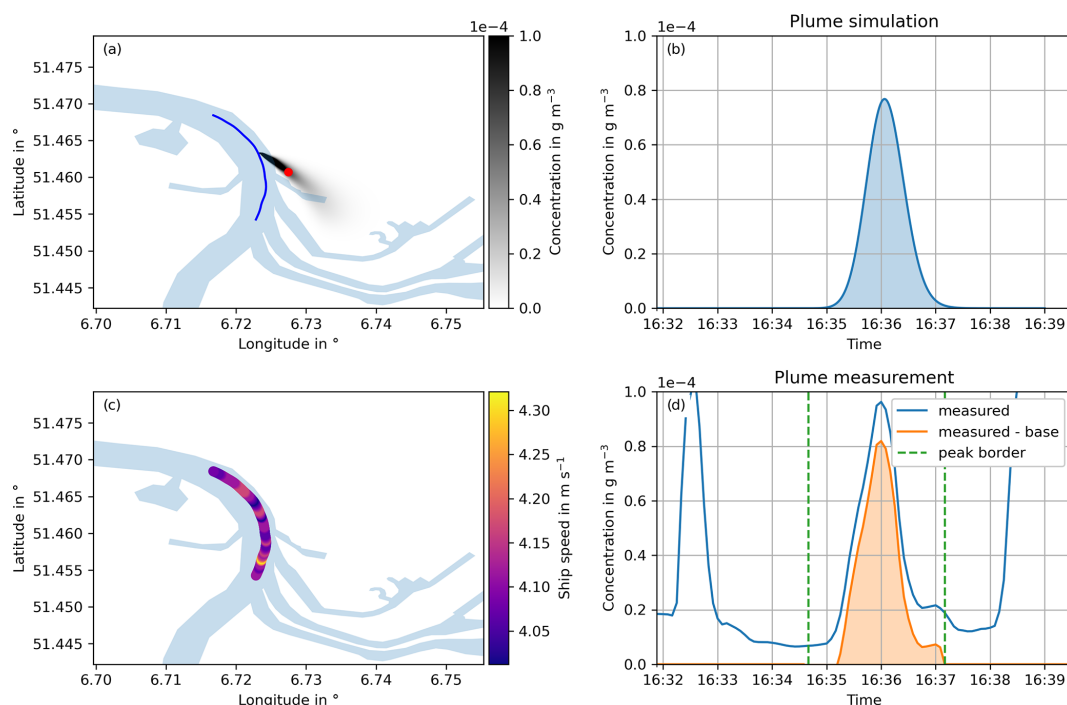


**Figure 4.** An example of a plume simulation for 22 August 2018 at 16:36 UTC compared with the measured plume. **(a)** A map of the modelled plume for the time when the highest concentration has been measured. **(b)** A plot of the simulated concentration of NO<sub>x</sub> at the measurement site as a function of time. **(c)** A map showing the ship speed over ground for each time step. **(d)** A plot of the measured NO<sub>x</sub> concentration as a function of time at the measurement station. The blue line represents the NO<sub>x</sub> concentration, and the orange line is the background-corrected NO<sub>x</sub> concentration of the peak.

measurement site. The parameters varied are wind speed, wind direction, atmospheric stability, and the position of the ship in longitude, latitude, and height. Each of these parameters is changed within the uncertainty ranges given in Table 2 (an example can be found in Appendix C). For each changed parameter, the derived integrated peak concentrations are then compared to the integrated peak concentration of the reference simulation. The resulting concentrations of a set of Monte Carlo simulations are then summarised by the mean value ( $\text{mean}_{C_j}$ ), the standard deviation ( $\sigma_{C_j}$ ), and the minimum ( $\text{min}_{C_j}$ ) and maximum value ( $\text{max}_{C_j}$ ). These values are compared to the reference simulation of the unperturbed input parameters. To be evaluated further, the following five criteria must be met by the set of Monte Carlo simulations for each input parameter:

1.  $\text{mean}_{C_j}/C_{\text{model}}$  must be between 0.5 and 1.5 to eliminate cases with a systematic deviation caused by the uncertainty in a single input;
2.  $\sigma_{C_j}/C_{\text{model}}$  must be lower than or equal to 1 to eliminate cases with a high variability caused by the uncertainty in a single input;
3. the difference between  $\text{min}_{C_j}/C_{\text{model}}$  and  $\text{max}_{C_j}/C_{\text{model}}$  must be smaller than 2 to eliminate cases with a large spread between the minimum and

maximum of the set due to the uncertainty in a single input;

4. the absolute error in the derived emission rate must be lower than  $5 \text{ g s}^{-1}$ , which eliminates cases in which the uncertainty is of a larger order of magnitude than the emission rate; and
5. the relative error in the derived emission rate must be smaller than 200 %, which eliminates cases in which the uncertainty is much larger than the emission rate.

### 3.5 Uncertainty in the NO<sub>x</sub> emission rates

In this section, we investigate the uncertainty in the measurement. This is considered to be the standard error in the emission rate, i.e. 1 standard deviation of the distribution of emission rates. The uncertainty in the derived emission rate is given by the following:

$$\sigma_Q = \sqrt{\left(\frac{\partial Q_{\text{meas}}}{\partial C_{\text{meas}}} \cdot \sigma_{C_{\text{meas}}}\right)^2 + \left(\frac{\partial Q_{\text{meas}}}{\partial C_{\text{model}}} \cdot \sigma_{C_{\text{model}}}\right)^2}, \quad (3)$$

where  $\sigma_{C_{\text{meas}}}$  is the uncertainty in the measured integrated peak trace gas concentration, and  $\sigma_{C_{\text{model}}}$  is the uncertainty

**Table 2.** Uncertainties in the input parameters used in the Monte Carlo simulations.

Abbreviation	Name	Calculation of value
$\sigma_{\text{long}}$	Source position longitude	Uncertainty in the AIS signal, 10 m
$\sigma_{\text{lat}}$	Source position latitude	Uncertainty in the AIS signal, 10 m
$\sigma_H$	Plume height	$\sqrt{\sigma_{\text{fh}}^2 + \sigma_{\text{wl}}^2}$
$\sigma_{\text{fh}}$	Funnel height	Estimated at 5 m
$\sigma_{\text{wl}}$	Water level	Mean high water level – mean low water level
$\sigma_U$	Wind speed	Standard deviation of the wind speed
$\sigma_\theta$	Wind direction	Estimated at 10°
$\sigma_{\text{stability}}$	Stability	Atmospheric dispersion parameters of class with lower stability and higher stability than the assigned class
$\sigma_{\text{Cmeas}}$	Uncertainty in the measured peak area	$\sqrt{\text{SD}(\text{peak})^2 \cdot n}$ , where $n$ is the number of nodes used to calculate the peak area

in the modelled integrated peak trace gas concentration. The uncertainty in the model is defined as follows:

$$\sigma_{C_{\text{model}}} = \sqrt{\sigma_{C_U}^2 + \sigma_{C_\theta}^2 + \sigma_{C_{\text{stability}}}^2 + \sigma_{C_{\text{long}}}^2 + \sigma_{C_{\text{lat}}}^2 + \sigma_{C_H}^2}, \quad (4)$$

where each  $\sigma_{C_j}$  is the standard deviation of the modelled trace gas concentrations of the Monte Carlo simulations with respect to changes in an individual input parameter ( $j$ ). In the Monte Carlo simulations, each parameter is varied individually, i.e. independently. The consequences of the changes in more than one parameter at a time are assumed to be negligible. The largest sources of uncertainty in the derived emission rate are the wind speed, wind direction, and stability. Wind speed and wind direction influence the shape and the time of appearance of the modelled peak. The area of the peak changes as a function of wind speed, and lower wind speeds lead to a larger peak, while higher wind speeds lead to a smaller peak. The peaks also shift in time. With lower wind speeds than assumed, the modelled plume arrives at the measurement site later than expected, while with higher-than-assumed wind speeds, it arrives too early. The wind direction has a similar effect and also changes the peak area and the time of arrival of the peak maximum. Stability, however, only changes the modelled peak area; more unstable conditions lead to smaller modelled peaks, as the plume can also grow vertically, and the pollutants are dispersed over a larger volume. In contrast, more stable conditions lead to larger modelled peaks, as the vertical dispersion is hindered. The source position does not play such an important role, and the changes in latitude, longitude, or height do not show significant changes in the modelled peak within the considered uncertainties. Also, the resulting uncertainty within the measured peak area is small compared to the uncertainty caused

by the wind speed, wind direction, and stability. An example of the Monte Carlo simulations and the respective influence on the modelled peaks can be found in Fig. C1.

## 4 Results

At DURH, more than 291 000 ship passages were identified in the AIS signals. For 32 900 ship passages, peaks have been identified and could be assigned to specific source ships. For 23 500 of those peaks, it was possible to determine the NO<sub>x</sub> emission rate, which fulfils the criteria of the quality control described previously. At NERH, 5500 peaks have been identified, and the respective emission rates have been derived. In 3200 cases, those derived NO<sub>x</sub> emission rates fulfil the quality criteria. The number of identified ship plumes is mainly limited by the wind, as the wind is needed to transport the emitted pollutants towards the measurement site. An additional limitation is the traffic density, as in situations of high traffic, an unambiguous identification of a ship plume is often not possible.

### 4.1 DURH

The derived emission rates were then summarised in the context of the respective CEMT (European Conference of Ministers of Transport) ship class (Table 3), the direction of travel (upstream or downstream), and their speed over ground (e.g. Fig. 5). The majority of ships belong to ship classes IV, Va, Vb, and Jowi, which together account for approximately 80 % of the total ship traffic (Fig. 6). Between 2017 and 2021, there were approximately 256 ship passages each day. As can be seen in Fig. 7, the majority of ships travelling upstream have a speed over ground of about 3 m s<sup>-1</sup>, while

**Table 3.** Modified ship classification scheme based on CEMT (European Conference of Ministers of Transport, 1992) classes. Ships are categorised by their respective length and width; e.g., a ship longer than 86 m but shorter than 111 m and width between 10 and 12 m is classified as class Va. Additionally, coupled units are identified via their Electronic Reporting International (ERI) code, which is also transmitted in the AIS signals.

Class	Maximum length (m)	Maximum width (m)	Cargo capacity (t)
I	39	6	350
II	56	7	655
III	68	9	1000
IV	86	10	1350
Va	111	12	2750
Vb	136	12	4000
Jowi	136	18	5300
VIa	173	12	5500
VIb	194	23	11 000
VIc	194	35	16 500
Coupled unit (C-U)	Motor freighter pushing one barge identified via the ERI identifier		
Unknown	Ships without information about width and/or length		

the majority of ships travelling downstream have speeds over ground of about  $5 \text{ m s}^{-1}$ .

For the most common ship classes, this enables the NO<sub>x</sub> emission rates of the respective class under real sailing conditions to be characterised. For less common ship classes, there are fewer observations, which leads to a higher uncertainty in the summarised NO<sub>x</sub> emission rates for these classes. In addition, there might not be enough data to differentiate sufficiently between the direction of travel or different speeds. The speed over ground is correlated with the emission rates, with higher speeds leading to higher emissions, as expected (e.g. Fig. 8).

Furthermore, the direction of travel is important when investigating the emissions for a given speed. Ships that travel upstream have to overcome the river current and therefore need more power to achieve the same speeds over ground compared to ships travelling downstream. With the same speed in water, the engine-operating conditions should be similar to and independent of the direction of travel. Consequently, we assume that the NO<sub>x</sub> emission rates are similar. A direct comparison for ship classes IV, Va, Vb, and Jowi shows that ships travelling upstream with a speed of about  $3 \text{ m s}^{-1}$  and ships travelling downstream with a speed of  $5 \text{ m s}^{-1}$  have similar NO<sub>x</sub> emission rates in their respective size class (shown in Table 5), which suggests similar operating conditions.

Unfortunately, at the DURH station, most of the identified ships are vessels which are travelling upstream. Out of the 23 500 quality-checked emission rates, approximately 13 500 are emitted by ships travelling upstream, approximately 3400

are from ships travelling downstream, and 6500 changed their direction within the modelled time frame, i.e. to enter or leave DURH or take a further connection to a channel. The main wind direction at DURH is southwesterly, which is parallel to the river, and ship plumes are therefore transported along the river. Unambiguous assignment is only possible if there is just a single ship plume that can reach the measurement station. Ships travelling upstream need a longer time to pass through the area, as they are slower than ships travelling downstream. Therefore, in cases of high traffic density, the longer time window of the ships travelling slower upstream increases the chances of an unambiguous identification and results in a larger number of observed ship plumes for that particular direction.

The NO<sub>x</sub> emission rates in the context of size (or ship class) are more difficult to summarise (see Fig. 5). Generally, larger ships show larger NO<sub>x</sub> emission rates than smaller ships. Larger ships usually have more powerful engines to provide the power needed to move and manoeuvre the ship. More powerful and larger engines consume more fuel and therefore have higher emission rates than smaller engines. At the same time, the larger ships are usually newer, and their emissions are regulated, while older ships are subject to grandfathering, which means that their engines do not have to comply with new regulations. The new regulations are only applicable if the engine of an older ship is exchanged. Due to the long service life of inland ships, many of the smaller ships do not fall under the regulations and therefore still have high emissions.

#### 4.1.1 Comparison with on-board emission measurements

In order to validate the emission rates within the CLINSH project, a comparison has been carried out between the values derived here from onshore observations of the CLINSH fleet and the respective on-board measurements. CLINSH ships have been identified using the AIS signal, as described in Sect. 3. For the NO<sub>x</sub> plumes from shipping, which passed the quality control criteria, the CLINSH data were searched to identify whether on-board data are available for the same time interval. For the case of a match, on-board data have been averaged for the period in which the plume detected by the onshore observation system was released by the ship. As the uncertainty in the Gaussian puff model is quite high, data 1 min before and after the release time were included in the plume average to take this into account. The 16 different CLINSH ships were observed nearly 200 times with both on-board and onshore measurement systems. Table 4 and Fig. 9 give a summary of the results obtained.

For almost half of the ships, the agreement between on-board and onshore observations is good and well within the error bars. However, it turns out that, for some ships (e.g. ship M), onshore values are systematically higher than the on-board data for the same time. One possible explana-

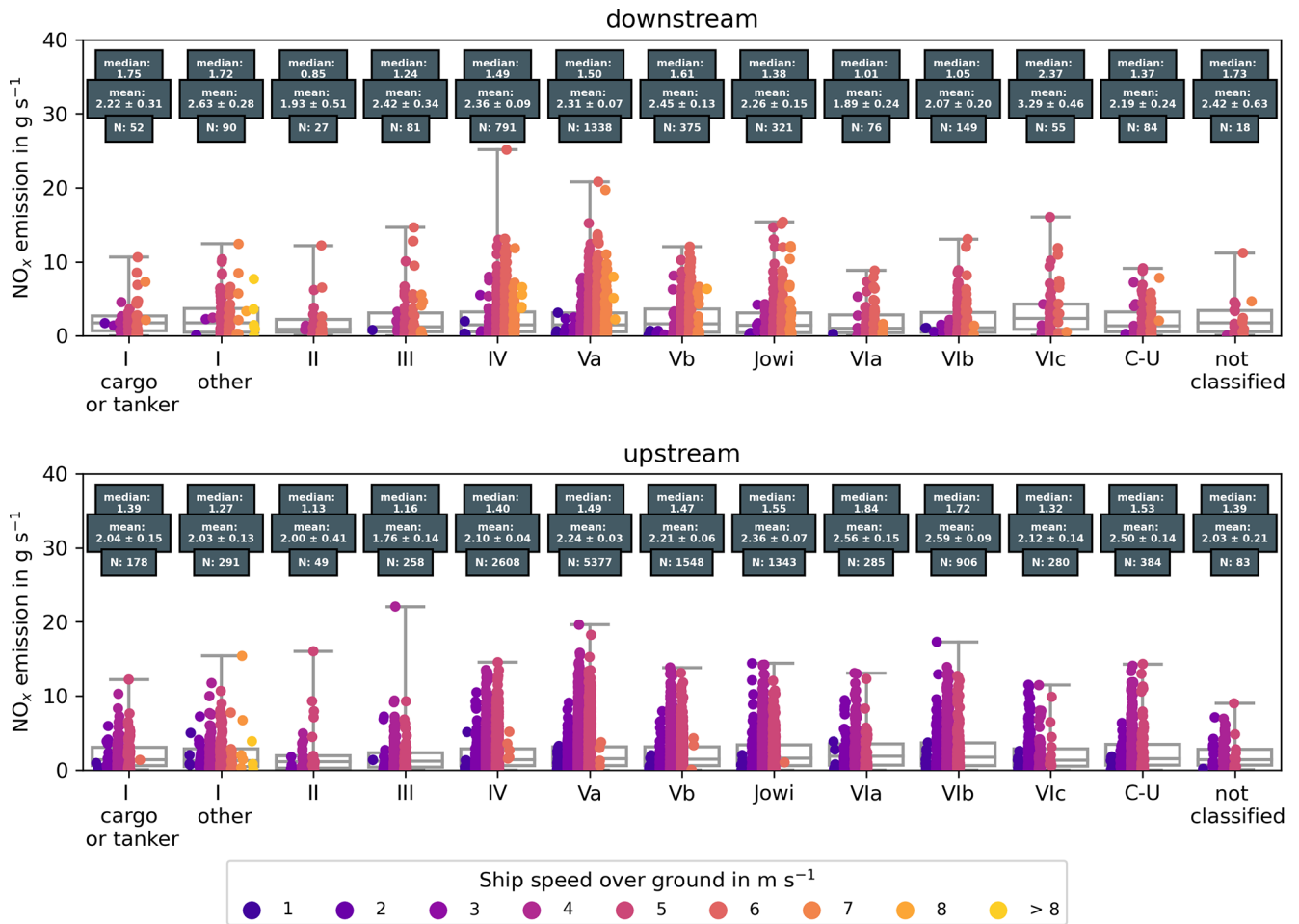


**Figure 5.** NO<sub>x</sub> emission rates for all ship classes, as derived from measurements at DURH. Single measurements are colour coded to the respective mean ship speed during the measurement.

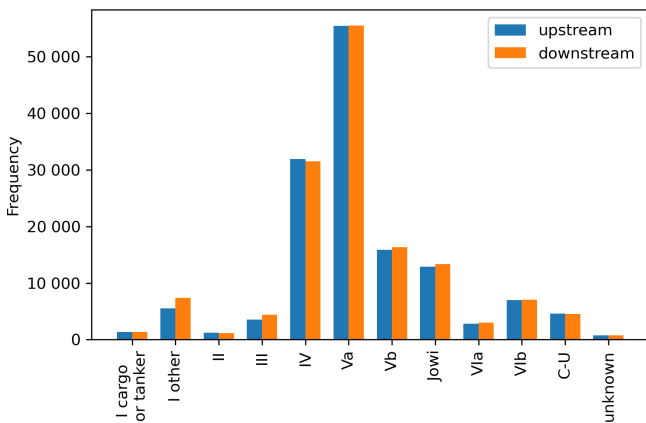


**Figure 6.** Ship traffic and fleet composition at DURH between November 2017 and December 2021. In total, 291 635 ship passages have been identified.

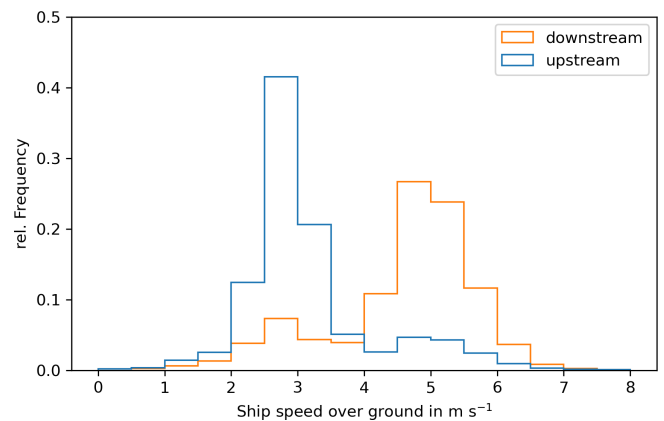


**Figure 7.** Ship speed over ground for all ship passages identified at DURH as a function of direction of travel.

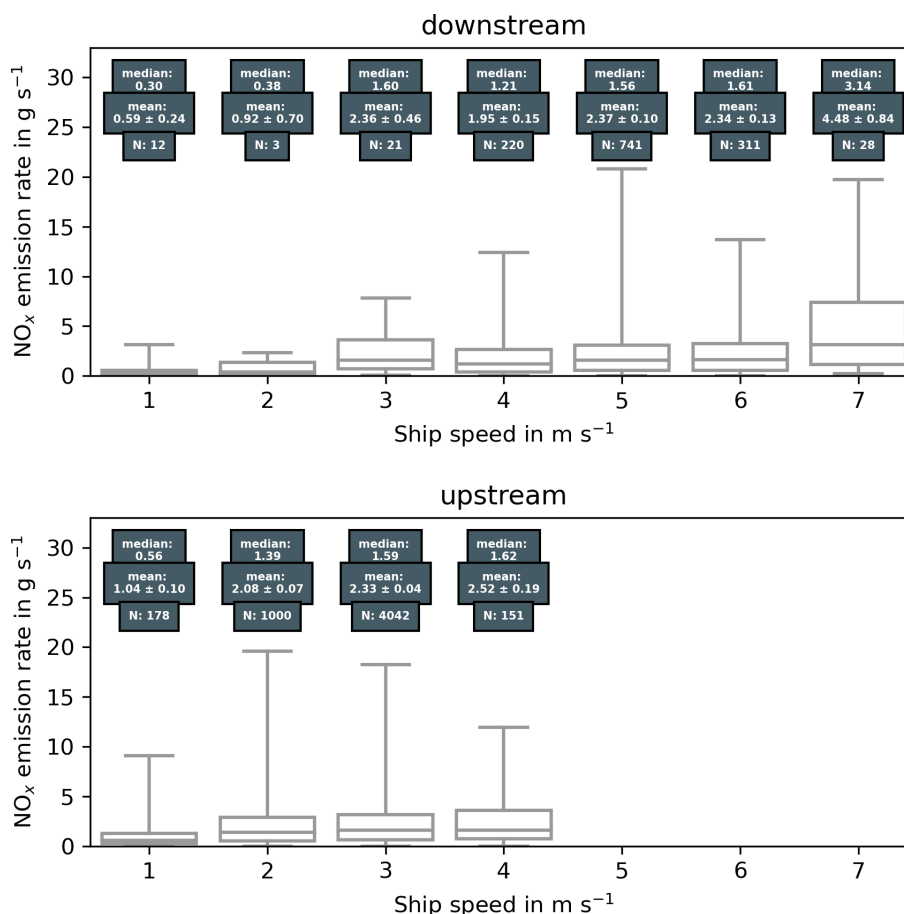


**Figure 8.** NO<sub>x</sub> emission rates for ship class Va and their dependence on the direction of travel and ship speed over ground, as derived from data measured at DURH.

tion is that some ships use more than one main engine for navigation, but the on-board measurement systems usually only capture the emissions of one of the engines and not the total amount emitted at the stack. The total emission rate for all main engines is assumed to be the number of engines multiplied by the measured on-board emission rates. In addition, some vessels also use auxiliary engines to power generators or bow thrusters, which also add to the total emissions of the ship and can be seen by the onshore measurements but not the on-board measurements. Taking into account all ships and all simultaneous observations, the ratio between onshore and on-board measurements is about  $1.3 \pm 0.1$  (see Fig. 9). Additionally, ship M is equipped with a SCR (selective catalytic reduction) system to reduce the NO<sub>x</sub> emissions, which did not always operate.

#### 4.1.2 Comparison with other studies

The emission behaviour of vessels is usually described and evaluated by emission factors. These emission factors are relative measures; e.g. the amount of emitted NO<sub>x</sub> is expressed per unit of burnt fuel or per amount of power generated by

the engine. The absolute emission rate of NO<sub>x</sub> has to be calculated from the emission factors and additional information about the fuel consumption. For comparison with the emission factors derived in other studies, two fuel consumption scenarios are considered. In the first scenario, a fuel consumption of  $108 \text{ kg h}^{-1}$  is assumed, which describes the fuel consumption of a ship with 3200 t cargo capacity travelling downstream. The second scenario uses a fuel consumption of  $162 \text{ kg h}^{-1}$ , which describes the fuel consumption of a ship with 3200 t cargo capacity travelling upstream against the current. Both scenarios are based on the specific fuel consumption levels (in  $\text{kg km}^{-1}$ ), which are  $6 \text{ kg km}^{-1}$  for ships travelling downstream and  $15 \text{ kg km}^{-1}$  for ships travelling upstream (Allekotte et al., 2020). The specific fuel consumption has been converted (to  $\text{kg h}^{-1}$ ), using the average speed over ground for ships travelling upstream and downstream, which is 3 and  $5 \text{ m s}^{-1}$ , respectively.

Table 5 shows the comparison of the values in the literature applied to these two scenarios with the emission rates derived in this study. The lower fuel consumption scenario shows absolute NO<sub>x</sub> emission rates between 1.17 and  $1.71 \text{ g s}^{-1}$ . The higher fuel consumption scenario shows emission rates from

**Table 4.** Comparison of NO<sub>x</sub> emission rates derived from onshore measurements and on-board measurements for different ships participating in the CLINSH project. The number of engines only includes the main engines used for navigation, and on-board measurements were only carried out on one of them. The number of engines used on ship G is not known but assumed to be 1.

Ship	Class	No. of engines	Onshore mean (g s <sup>-1</sup> )	Onshore median (g s <sup>-1</sup> )	Onshore SD (g s <sup>-1</sup> )	On-board mean (g s <sup>-1</sup> )	On-board SD (g s <sup>-1</sup> )	<i>n</i>
A	III	1	0.84	0.84	0.27	1.23	0.34	2
B	IV	1	0.94	0.40	0.92	0.81	0.32	6
C	IV	1	2.20	1.66	1.29	1.34	0.51	6
D	Va	1	2.12	1.75	0.63	0.73	0.41	3
E	Va	1	0.56	0.56	–	0.42	0.14	1
F	Va	1	2.40	1.55	2.33	2.17	0.67	45
G	Va	?	1.89	1.77	0.71	1.53	0.32	5
H	Va	1	3.65	3.85	2.44	2.47	1.23	4
I	Jowi	1	1.63	1.77	0.88	1.13	0.32	4
J	Jowi	1	2.05	0.30	3.86	0.71	0.41	13
K	Jowi	1	1.58	1.30	1.10	0.92	0.43	14
L	C-U	1	1.43	0.74	1.49	0.35	0.16	7
M*, **	III	2	2.15	1.70	2.24	0.65 (1.30)	0.43 (0.86)	13
N*	Va	3	1.73	0.98	1.81	0.61 (1.83)	0.32 (0.96)	9
O*	Jowi	2	1.56	0.75	2.08	0.72 (1.44)	0.39 (0.78)	25
P*	VIb	2	1.44	0.66	1.37	0.83 (1.66)	0.42 (0.84)	17

\* Ships M, N, O, and P are equipped with more than one main engine used for navigation. It is assumed that the NO<sub>x</sub> emission rates for all engines are the same. The total emission rate for all main engines is therefore assumed to be the number of engines multiplied by the measured on-board emission rates (shown in parentheses).

\*\* Ship M is equipped with a selective catalytic reduction (SCR) system to reduce the NO<sub>x</sub> emissions, which was not always operational.

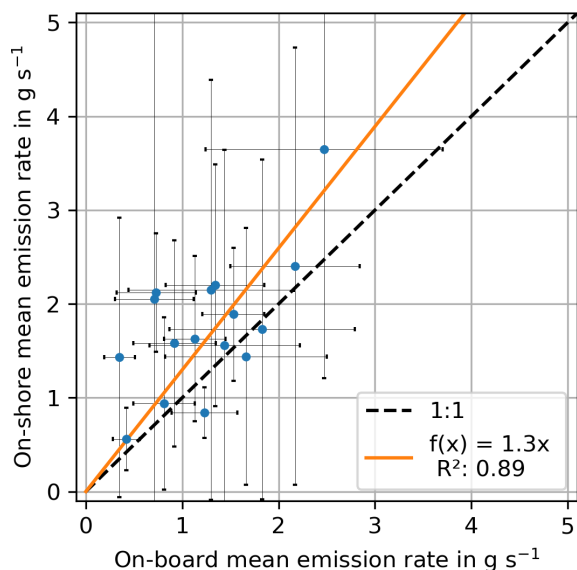


**Figure 9.** Scatterplot of on-board and onshore emission rates. Each dot represents the mean value for one ship, and error bars indicate respective standard deviations. For ships with more than one main engine, the number of engines has been taken into account for the on-board emission rates (also see Table 4).

1.75 to 2.57 g s<sup>-1</sup>. In comparison, the mean NO<sub>x</sub> emission rates derived in DURH for ships that travel downstream with the most common speed of 5 m s<sup>-1</sup> are in the range of 2.36 to 2.53 g s<sup>-1</sup>. For ships travelling upstream with the most

common speed over ground of 3 m s<sup>-1</sup>, the NO<sub>x</sub> emission rates are 2.17 to 2.36 g s<sup>-1</sup>. Generally, the mean NO<sub>x</sub> emission rates fit into the range given by the emission factors of other studies but are at the upper limit of the given range. At lower speeds, the mean emission rates are also lower. At the most common speeds over ground in a given direction, the emission rates for ships travelling upstream and ships travelling downstream are similar. In general, the scenario with high fuel consumption seems to better reflect the derived emission rates. This indicates similar fuel consumption and engine operation scenarios for ships travelling downstream and ships travelling upstream. Assuming a water velocity of 1 m s<sup>-1</sup>, the average speed in water would be similar for both directions, which would also indicate similar engine operation conditions and therefore similar emission rates.

#### 4.1.3 Comparison to current NO<sub>x</sub> regulations

Table 6 shows the regulations that are in place for ships newly built or that had their engine replaced in the specified years. The regulations are defined (in g kWh<sup>-1</sup>) and have been converted (to g kg<sup>-1</sup>), using a specific fuel consumption of 230 g kWh<sup>-1</sup> (De Vlieger et al., 2004). The specific fuel consumption of ship engines can vary between different engines and also depends on the engine load, with a lower engine load generally increasing the specific fuel consumption (van Mensch et al., 2018). Measurements presented by van Mensch et al. (2018) show that the specific fuel consumption for different engines can reach about 290 g kWh<sup>-1</sup> for

**Table 5.** Comparison of the derived NO<sub>x</sub> emission rates (ERs; in g s<sup>-1</sup>) with the emission factors (EFs; in kg h<sup>-1</sup>) derived from other studies. To calculate the ERs from the EFs, two fuel consumption scenarios are evaluated. Both scenarios are based on specific fuel consumption values for ships with a cargo capacity of 3200 t (approximately class Va and Vb). First, a fuel consumption of 108 kg h<sup>-1</sup> is assumed for ships that travel downstream, and second, a fuel consumption of 162 kg h<sup>-1</sup> is assumed for ships travelling upstream.

Study	NO <sub>x</sub> EF (g kg <sup>-1</sup> )	NO <sub>x</sub> ER (g s <sup>-1</sup> ) 108 kg h <sup>-1</sup>	NO <sub>x</sub> ER (g s <sup>-1</sup> ) 162 kg h <sup>-1</sup>
Trozzi and Vaccaro (1998)	51	1.53	2.30
Kesgin and Vardar (2001)	57	1.71	2.57
Klimont et al. (2002)	51	1.53	2.30
Rohács and Simongáti (2007)	47	1.41	2.12
Schweighofer and Blaauw (2009)	39	1.17	1.75
van der Gon and Hulskotte (2010)	45	1.35	2.03
Diesch et al. (2013)	53	1.59	2.39
Knörr et al. (2013)	49	1.47	2.21
Kurtenbach et al. (2016)	54	1.62	2.43
Kattner (2019)	41	1.23	1.85
This study (DURH)		Downstream	Upstream
Speed over ground		5 m s <sup>-1</sup>	3 m s <sup>-1</sup>
IV	–	2.36 ± 0.13	2.17 ± 0.05
Va	–	2.37 ± 0.10	2.33 ± 0.04
Vb	–	2.53 ± 0.17	2.35 ± 0.07
Jowi	–	2.26 ± 0.19	2.36 ± 0.08

**Table 6.** Overview of NO<sub>x</sub> emission limits, according to CCNR (The European Parliament and the European Council, 1998; CCNR, 2020) and EU regulations (given, in both cases, in units of g kWh<sup>-1</sup>; The European Parliament and the European Council, 2016). For comparison, these have been converted (to g kg<sup>-1</sup>) using a specific fuel consumption for inland ships of 230 g kWh<sup>-1</sup> (De Vlieger et al., 2004) and further converted (eventually to g s<sup>-1</sup>) using the 162 kg h<sup>-1</sup> fuel consumption scenario.

Regulation	In effect since	Engine power (kW)	NO <sub>x</sub> EF (g kWh <sup>-1</sup> )	NO <sub>x</sub> EF (g kg <sup>-1</sup> )	NO <sub>x</sub> ER (g s <sup>-1</sup> )
CCNR I	2002	$P > 130$	9.2	39.9	1.80
CCNR II	2007	$P > 130$	6.0	26.1	1.17
EU RL2016/1629	2019	$130 < P < 300$	2.1	9.1	0.41
EU RL2016/1629	2019	$P > 300$	1.8	7.8	0.35

engine loads below 20 % and can reach between 200 and 230 g kWh<sup>-1</sup> for engine loads higher than 20 %. Additionally, the specific fuel consumption also depends on the age of the engine, as newer engines generally have a lower specific fuel consumption (De Vlieger et al., 2004). To interpret the derived NO<sub>x</sub> emission rates in the context of these regulations, the limits given in the regulations were converted (to g s<sup>-1</sup>) using the 162 kg h<sup>-1</sup> fuel consumption scenario. These values then can be interpreted as an upper limit for the NO<sub>x</sub> emission rates for cases of high fuel consumption. Figure 10 shows the NO<sub>x</sub> emission rates derived from the onshore measurements at DURH for the most common ship classes (VI, Va, Vb, and Jowi) as a function of their respective speed over ground. For all ship classes, the mean NO<sub>x</sub> emission rates for speeds higher than 2 m s<sup>-1</sup> exceed even the least strict regulation (CCNR I) of 9.2 g kWh<sup>-1</sup>. For speeds over ground lower than 3 m s<sup>-1</sup>, the mean NO<sub>x</sub> emission rates are within

the CCNR I limit. But in these cases, the assumed high fuel consumption scenario usually does not apply. When looking at the individual ship passages for the classes IV, Va, Vb, and Jowi, approximately 50 % of the derived NO<sub>x</sub> emission rates plus their respective uncertainty ( $Q_{\text{meas}} + \sigma_Q$ ) are below the CCNR I upper limit, approximately 40 % are below CCNR II, and 16 % are below EU RL2016/1629. These results indicate that a large number of old ships with unregulated engines are still in operation.

Kurtenbach et al. (2016) reported emission factors of 20 to 161 g kg<sup>-1</sup>, with an average of  $52 \pm 3$  g kg<sup>-1</sup>, while Kattner (2019) derived a mean emission factor of  $41 \pm 28$  g kg<sup>-1</sup>. In both studies, the mean emission factor is above the limits given by the regulations, but here individual ships also already comply with the regulations.

In addition, it has to be kept in mind that the water level, hull form, and propeller configuration can have a significant

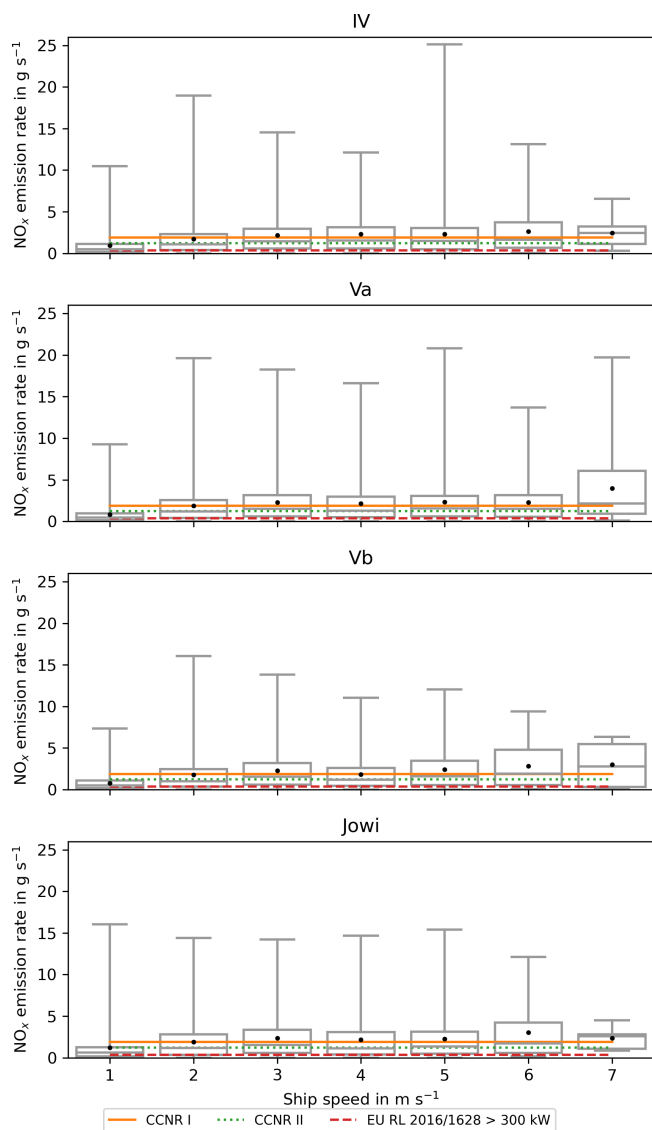


**Figure 10.** Box plots of NO<sub>x</sub> emission rates for ship classes IV, Va, Vb, and Jowi as a function of ship speed over ground, as derived from data measured at DURH. The mean value is shown as a black dot and the median value as a grey line. The limits given by the CCNR I, CCNR II, and EU RL2016/1628 regulations were converted (from gkWh<sup>-1</sup> to g s<sup>-1</sup>) and are shown as lines (see Table 6 for more details).

influence on the power required to navigate a ship and, therefore, on the number of emitted pollutants (Friedhoff et al., 2018). The mean NO<sub>x</sub> emission rates presented here are the result of the evaluation of several years and thousands of different ships. It is therefore expected that the mean values are representative of the average ship emissions on the Rhine at the DURH measurement site.

In addition to the regulation of new ships and engines, additional technical measures, such as exhaust gas aftertreatment, can be used to reduce the emissions caused by ship

traffic. The capabilities of exhaust gas aftertreatment systems have already been discussed in previous studies (e.g. Schweighofer and Blaauw, 2009; Kleinebrahm and Bourbon, 2013; Pirjola et al., 2014; Brandt and Busch, 2017; Busch et al., 2020).

## 4.2 NERH

As the NERH measurement site is located directly within the harbour area, the ships here are generally slower and show lower NO<sub>x</sub> emission rates compared to the DURH measurement site (e.g. Fig. 11). As there is no strong river current, ships have been classified into ships leaving the harbour and ships entering the harbour, instead of ships travelling upstream or downstream. Generally, ships show similar emission rates independent of their leaving or entering the harbour area (e.g. Fig. 12).

## 4.3 Ideal measurement location

The improved algorithm presented here has several advantages over the method described in Krause et al. (2021), where a Gaussian plume model was used to derive NO<sub>x</sub> and SO<sub>2</sub> emission rates from long-path DOAS measurements. An in situ station is easier to model than a remote sensing site because the concentration is only measured at the location of the station and does not represent the integrated column of an absorber along a light path. The equipment used in this study can be found in standardised air quality measurement stations, facilitating the use of existing stations for ship emission estimates. Only the additional AIS receiver is needed to provide information about the passing vessels. This means that NO<sub>x</sub> emission rates can be derived from existing stations with fewer additional costs. In addition, in situ measurement stations are able to measure NO and NO<sub>2</sub> simultaneously so that NO<sub>x</sub> can be measured directly and does not need to be inferred from NO<sub>2</sub> observations, as in Krause et al. (2021).

The measurement stations in DURH and NERH were both suitable locations to derive emission rates from passing vessels under real sailing conditions. However, their locations are not ideal and increase the difficulty when applying the algorithm to the measurement data. At the time of the installation of the measurement sites, the derivation of onshore emission rates was not the focus of the CLINSH project. Consequently, we consider that the optimisation of the position of the measurement can improve the derivation of the emission rates and lower its uncertainty.

Ideally, a measurement station would be located at a section of a river where there are no confluences. This helps in the analysis of the derived emission rates, as it is easier to distinguish between ships travelling upstream and downstream. Also, it removes possible special manoeuvres carried out by the ships trying to enter or leave a confluence. Furthermore, the measurement station should be located at a straight river section, preferably with the main wind direction orthog-

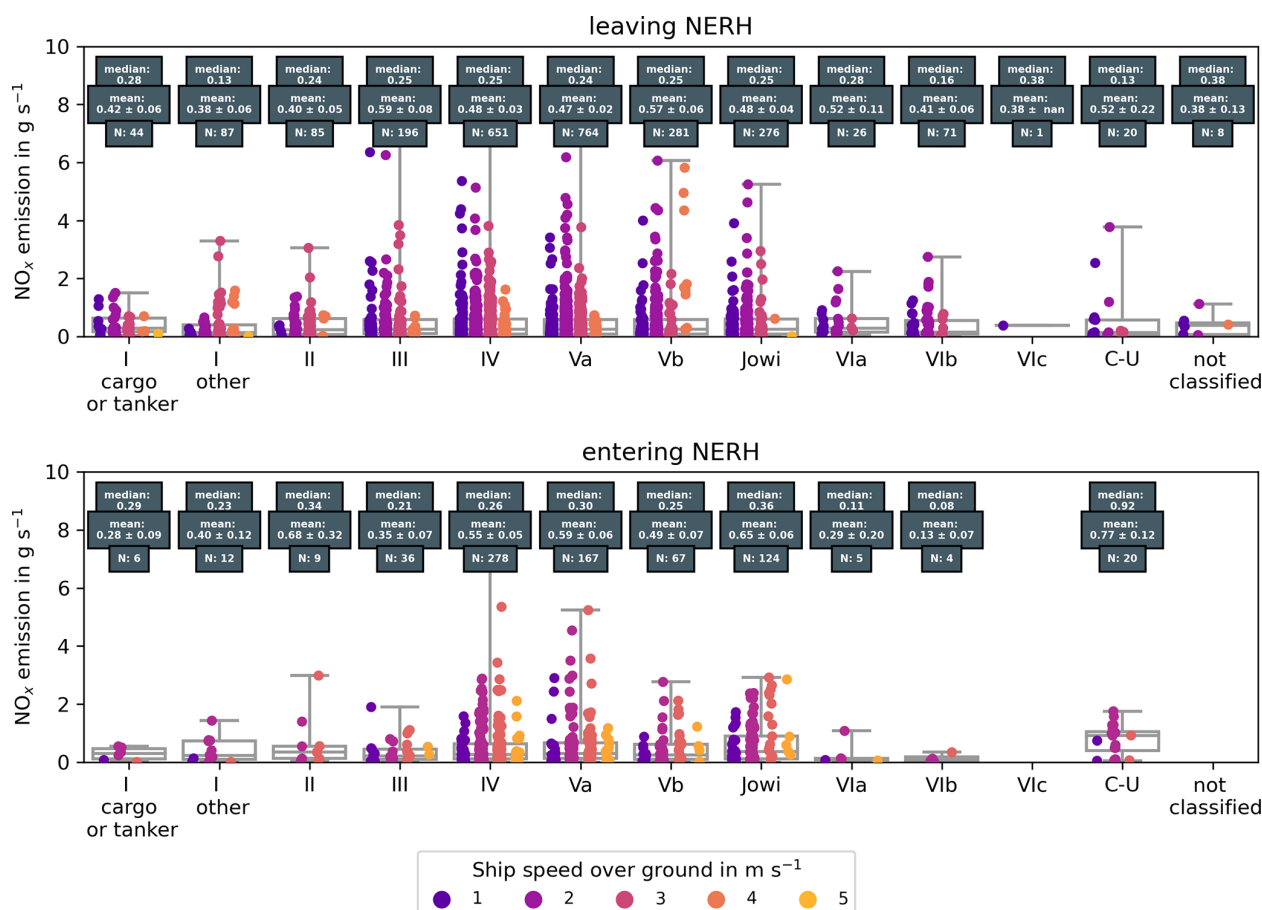


**Figure 11.** NO<sub>x</sub> emission rates for all ship classes, as derived from measurements at NERH. Single measurements are colour coded to the respective mean ship speed during the measurement.

onal to the river. This decreases the chances of overlapping plumes and therefore increases the chances of identifying the source ship. Locations where the wind blows along the river should be avoided because the plumes of several ships can be mixed, and the identification of the source ships can become impossible, especially when there is high traffic. Locations with point sources of NO<sub>x</sub> upwind of the measurement site should also be avoided. These point sources could cause additional peaks, mix with the ship plumes, and alter their respective peaks in the measured time series or simply lead to a highly variable background concentration which might be hard to correct. The terrain around the measurement site should be flat and even so that the surface roughness can be characterised easily. In summary, a simple geometry of the surroundings and a low number of obstacles (i.e. trees and buildings) are beneficial when using the Gaussian puff model. In addition, usage of measurements of the current water level would be beneficial because the uncertainty in the height of the emission could be reduced. Incoming solar radiation and cloud cover should ideally be measured at the measurement site to reduce the uncertainty regarding these parameters.

These suggestions about making emission measurements are not required for the derivation of emission rates, as has been shown in this study, but using them will improve the accuracy of future measurements.

## 5 Conclusions

As part of this study, two standardised in situ measurement stations have been set up to measure ship emissions on the river Rhine. The first was set up on the river shore in Duisburg (DURH) to measure the emissions directly at the Rhine, while the second one was installed in the harbour area of Neuss (NERH). The measurement stations were established in the period of September to October 2017. The station at DURH is still active, while the station at NERH made its planned measurements and was dismantled at the end of 2019. For both stations, it was possible to identify peaks in the measured NO<sub>x</sub> time series and find the corresponding source ships. A new method to derive absolute emission rates (in g s<sup>-1</sup>) from these peaks was developed and successfully applied to the data. Within the algorithm, each individual

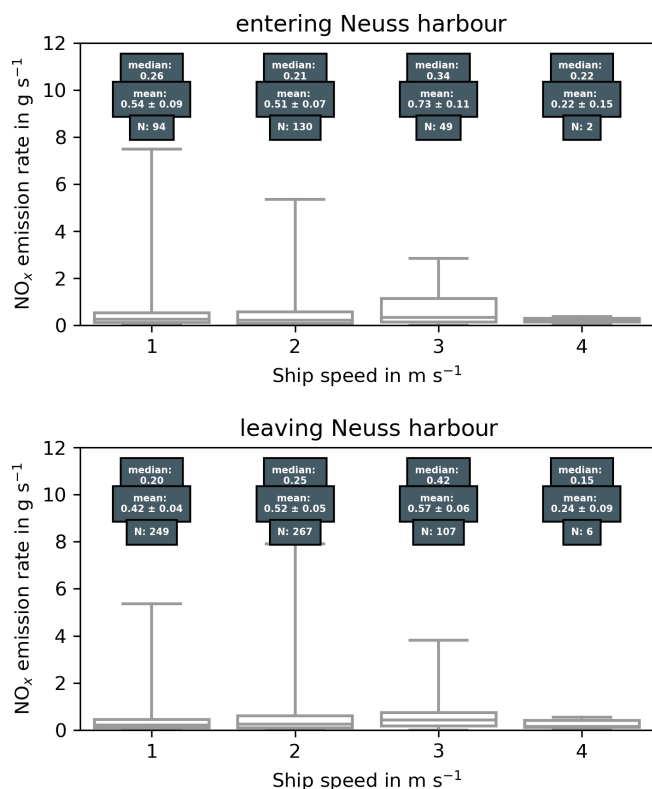


**Figure 12.** NO<sub>x</sub> emission rates for ship class IV and their dependence on the direction of travel and ship speed over ground, as derived from data measured at NERH.

ship passage is modelled by a Gaussian puff model, and the modelled concentration at the measurement site is compared to the measured concentration to calculate the emission rate. The modelled concentrations are quality controlled for non-physical results, which can occur when the uncertainty in the input parameters used in the Gaussian puff model is too high. At DURH, approximately 32 900 peaks have been identified and could be attributed to a source ship, and in approximately 23 500 cases, quality-controlled emission rates were derived. At NERH, approximately 5500 peaks have been identified, and approximately 3200 emission rates were derived. These emission rates were analysed in the context of ship class (size), speed over ground, and direction of travel (upstream and downstream). Generally, the emission rates increase with the ship size and ship speed; in addition, the emission rates of ships travelling upstream are higher than those of ships travelling downstream, but they have the same speed over ground.

The derived emission rates in this study have been compared to emission rates measured on board ships that participated in the project, and generally good agreement between both methods was found. Discrepancies can be explained by the different quantities that are measured. The onshore measurements represent the sum of all NO<sub>x</sub> emissions of the ship, including all auxiliary engines, while the on-board measure-

ments are only carried out on the main engine. For ships which use more than one engine for navigation, the on-board measurements were only realised for one engine and not for all of them. Therefore, the number of engines had to be considered for the comparison of onshore and on-board measurements. The emission rates have been compared to emission factors (in g kg<sup>-1</sup>) from other studies, under the assumption of two fuel consumption scenarios, and agree quite well, considering the uncertainties.

The mean emission rates for the most common ship classes (IV, Va, Vb, and Jowi) at speeds higher than 2 m s<sup>-1</sup> exceed even the least strict regulations of CCNR I of 9.2 g kWh<sup>-1</sup>. Looking at individual ship passages for these four classes, approximately 50 % comply with CCNR I, 40 % comply with CCNR II, and 16 % comply with EU RL2016/1629.

The algorithm mostly relies on input parameters that are routinely measured by standardised air quality stations; only additional information about the passing ships is needed and can be provided by AIS receivers. In contrast to emission factors, the derived emission rates can be directly used in conjunction with traffic statistics to model the total emissions caused by ship traffic in the area. This enables possible uncertainties caused by the assumptions made when converting the relative emission factors to absolute emission rates during the modelling process to be circumvented. In addition, the emission rates include the emission of all engines on board the ships and not only of the main engine for each passing vessel.

Generally, the derived emission rates should be representative of the Lower Rhine area, with similar streaming conditions to those encountered at the DURH measurement site. At the same time, evaluation of the AIS signals derived from DURH and NERH show that ships tend to adapt their speed to streaming conditions encountered at each measurement site, which could also influence their emission rates.

The emission rates collected in 2017–2021 have already been applied by LANUV for the port areas of DURH and NERH within the framework of CLINSH to calculate shipping-related emissions. It is planned to use this procedure for a future update of the inland waterway vessel emission register of the state of North Rhine-Westphalia for the determination of shipping emissions. The continuously measuring station at DURH will remain in operation in the coming years and will be evaluated using the described algorithm.

Appendix A: NO<sub>x</sub> emission rates at DURH**Table A1.** Summary of data shown in Fig. 5. NO<sub>x</sub> emission rates for ships travelling upstream are derived from measurements at DURH.

Class	Mean (g s <sup>-1</sup> )	Median (g s <sup>-1</sup> )	Min (g s <sup>-1</sup> )	Max (g s <sup>-1</sup> )	SD (g s <sup>-1</sup> )
Coupled unit (C-U)	2.50	1.53	0.001	14.31	2.75
I cargo or tanker	2.04	1.39	0.009	12.21	2.03
I other	2.03	1.27	0.006	15.4	2.27
II	2.0	1.13	0.007	16.04	2.9
III	1.76	1.16	0.003	22.07	2.2
IV	2.1	1.4	0.001	14.54	2.2
Jowi	2.36	1.55	0.001	14.4	2.44
VIa	2.56	1.84	0.001	13.09	2.59
VIb	2.59	1.72	0.001	17.31	2.7
VIc	2.12	1.32	0.004	11.5	2.35
Va	2.24	1.49	0.002	19.62	2.32
Vb	2.21	1.47	0.002	13.84	2.24
Not classified	2.03	1.39	0.031	9.0	1.9

**Table A2.** Summary of data shown in Fig. 5. NO<sub>x</sub> emission rates for ships travelling downstream are derived from measurements at DURH.

Class	Mean (g s <sup>-1</sup> )	Median (g s <sup>-1</sup> )	Min (g s <sup>-1</sup> )	Max (g s <sup>-1</sup> )	SD (g s <sup>-1</sup> )
Coupled unit (C-U)	2.19	1.37	0.054	9.12	2.18
I cargo or tanker	2.22	1.75	0.020	10.61	2.23
I other	2.63	1.72	0.007	12.41	2.70
II	1.93	0.85	0.085	12.2	2.65
III	2.42	1.24	0.004	14.64	3.04
IV	2.36	1.49	0.002	25.13	2.59
Jowi	2.26	1.38	0.0005	15.39	2.67
VIa	1.89	1.01	0.020	8.8	2.07
VIb	2.07	1.05	0.017	13.06	2.4
VIc	3.29	2.37	0.052	16.04	3.41
Va	2.31	1.50	0.003	20.81	2.52
Vb	2.45	1.61	0.001	12.04	2.49
Not classified	2.42	1.73	0.062	11.19	2.69

Appendix B: NO<sub>x</sub> emission rates at NERH**Table B1.** Summary of data shown in Fig. 11. NO<sub>x</sub> emission rates for ships entering NERH are shown.

Class	Mean (g s <sup>-1</sup> )	Median (g s <sup>-1</sup> )	Min (g s <sup>-1</sup> )	Max (g s <sup>-1</sup> )	SD (g s <sup>-1</sup> )
Coupled unit (C-U)	0.77	0.92	0.043	1.75	0.52
I cargo or tanker	0.28	0.29	0.009	0.54	0.22
I other	0.40	0.23	0.004	1.43	0.43
II	0.68	0.34	0.032	2.98	0.96
III	0.35	0.21	0.006	1.90	0.40
IV	0.55	0.26	0.001	7.48	0.81
Jowi	0.65	0.36	0.001	2.91	0.72
VIa	0.29	0.11	0.055	1.07	0.44
VIb	0.13	0.08	0.022	0.34	0.15
Va	0.59	0.30	0.001	5.24	0.83
Vb	0.49	0.25	0.006	2.76	0.60

**Table B2.** Summary of data shown in Fig. 11. NO<sub>x</sub> emission rates for ships leaving NERH are shown.

Class	Mean (g s <sup>-1</sup> )	Median (g s <sup>-1</sup> )	Min (g s <sup>-1</sup> )	Max (g s <sup>-1</sup> )	SD (g s <sup>-1</sup> )
Coupled unit (C-U)	0.52	0.13	0.001	3.77	0.97
I cargo or tanker	0.42	0.28	0.029	1.50	0.37
I other	0.38	0.13	0.0004	3.30	0.58
II	0.40	0.24	0.001	3.05	0.48
III	0.59	0.25	0.001	8.57	1.05
IV	0.48	0.25	0.0001	7.91	0.72
Jowi	0.48	0.25	0.003	5.24	0.70
VIa	0.52	0.28	0.061	2.25	0.54
VIb	0.41	0.16	0.007	2.75	0.52
Va	0.47	0.24	0.0004	7.02	0.69
Vb	0.57	0.25	0.001	6.06	0.92
Not classified	0.38	0.38	0.035	1.12	0.36

## Appendix C: Monte Carlo simulation

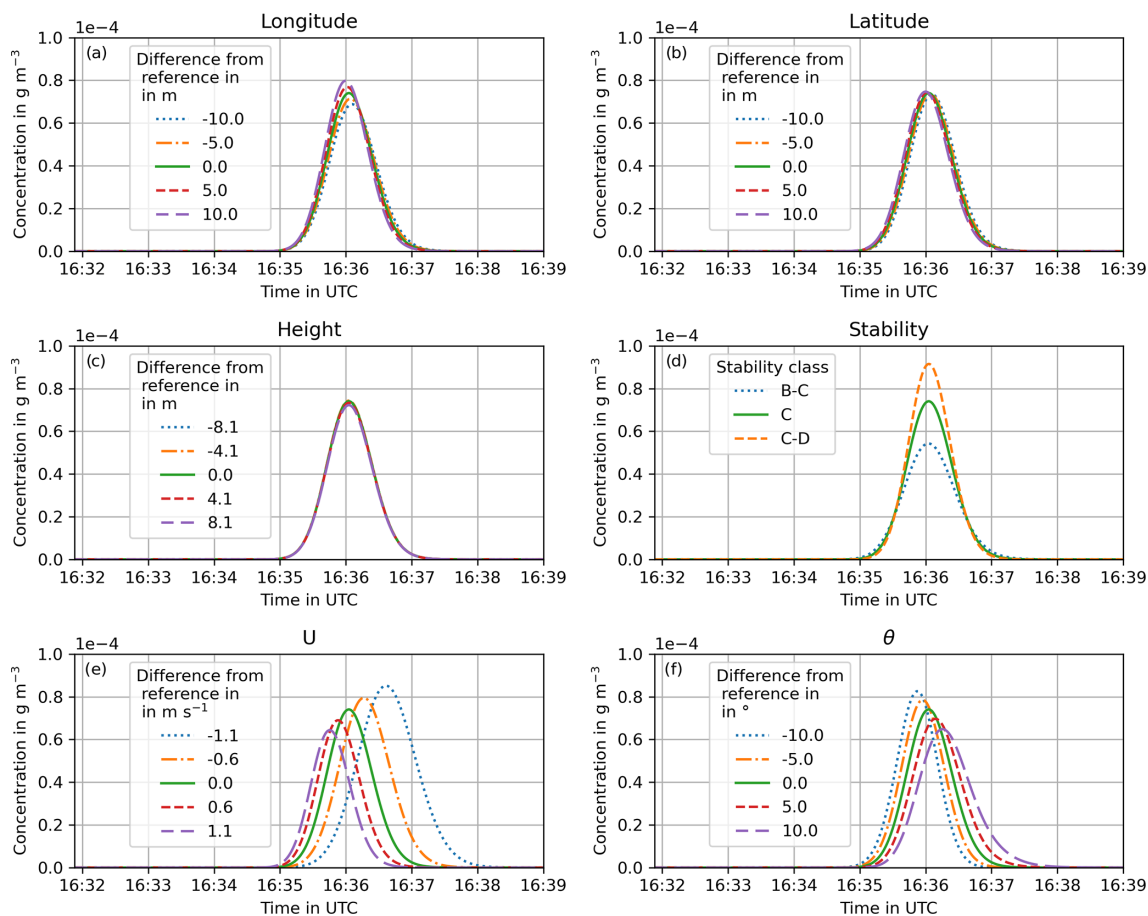


**Figure C1.** Monte Carlo simulations for the example plume shown in Fig. 4. In each plot, one parameter has been changed within its respective uncertainty, and the resulting model peaks are shown. The uncertainties shown in the plot legends are always expressed as a deviation from the reference simulation; e.g. in plot (a),  $-10$  m means that the ship positions have systematically been moved 10 m to the west, while 10 m means each position has been moved 10 m to the east. The reference simulation (no uncertainty) is shown as a solid green line.

*Code and data availability.* The data and code used in this study are available directly from the authors upon request. The derived  $\text{NO}_x$  emission rates can be found in the Supplement of this paper.

*Supplement.* The supplement related to this article is available online at: <https://doi.org/10.5194/amt-16-1767-2023-supplement>.

*Author contributions.* KK performed the analysis and wrote the paper, with input from FW, AR, DB, AB, JPB, SF, and OH. SF and OH were responsible for the measurements at the DURH and NERH measurement sites.

*Competing interests.* The contact author has declared that none of the authors has any competing interests.

*Disclaimer.* Publisher's note: Copernicus Publications remains neutral with regard to jurisdictional claims in published maps and institutional affiliations.

*Acknowledgements.* The research presented in this study has been funded in part by the EU LIFE project CLINSH and by the University of Bremen.

*Financial support.* The article processing charges for this open-access publication were covered by the University of Bremen.

*Review statement.* This paper was edited by Keding Lu and reviewed by Fan Zhou and one anonymous referee.

## References

- Alföldy, B., Lööv, J. B., Lagler, F., Mellqvist, J., Berg, N., Beecken, J., Weststrate, H., Duyzer, J., Bencs, L., Horemans, B., Cavalli, F., Putaud, J.-P., Janssens-Maenhout, G., Csordás, A. P., Van Grieken, R., Borowiak, A., and Hjorth, J.: Measurements of air pollution emission factors for marine transportation in SECA, *Atmos. Meas. Tech.*, 6, 1777–1791, <https://doi.org/10.5194/amt-6-1777-2013>, 2013.
- Allekotte, M., Biemann, K., Heidt, C., Colson, M., and Knörr, W.: Aktualisierung der Modelle TREMOD/TREMOD-MM für die Emissionsberichterstattung 2020 (Berichtsperiode 1990–2018), Umweltbundesamt, Dessau-Roßlau, ISSN 1862-4804, 2020.
- Ausmeel, S., Eriksson, A., Ahlberg, E., and Kristensson, A.: Methods for identifying aged ship plumes and estimating contribution to aerosol exposure downwind of shipping lanes, *Atmos. Meas. Tech.*, 12, 4479–4493, <https://doi.org/10.5194/amt-12-4479-2019>, 2019.
- Beecken, J., Mellqvist, J., Salo, K., Ekholm, J., and Jalkanen, J.-P.: Airborne emission measurements of SO<sub>2</sub>, NO<sub>x</sub> and particles from individual ships using a sniffer technique, *Atmos. Meas. Tech.*, 7, 1957–1968, <https://doi.org/10.5194/amt-7-1957-2014>, 2014.
- Beecken, J., Mellqvist, J., Salo, K., Ekholm, J., Jalkanen, J.-P., Johansson, L., Litvinenko, V., Volodin, K., and Frank-Kamenetsky, D. A.: Emission factors of SO<sub>2</sub>, NO<sub>x</sub> and particles from ships in Neva Bay from ground-based and helicopter-borne measurements and AIS-based modeling, *Atmos. Chem. Phys.*, 15, 5229–5241, <https://doi.org/10.5194/acp-15-5229-2015>, 2015.
- Berg, N., Mellqvist, J., Jalkanen, J.-P., and Balzani, J.: Ship emissions of SO<sub>2</sub> and NO<sub>2</sub>: DOAS measurements from airborne platforms, *Atmos. Meas. Tech.*, 5, 1085–1098, <https://doi.org/10.5194/amt-5-1085-2012>, 2012.
- Berkhout, A. J. C., Swart, D. P. J., van der Hoff, G. R., and Bergwerff, J. B.: Sulphur dioxide emissions of ocean-going vessels measured remotely with Lidar, RIVM Report 609021119/2012, National Institute for Public Health and the Environment, the Netherlands, <https://www.rivm.nl/bibliotheek/rapporten/609021119.pdf> (last access: 22 March 2023), 2012.
- Brandt, A. and Busch, D.: Emissionen des Containerschiffs „MS Aarburg,“: Auswirkungen der Nachrüstung mit einer Diesel-Wasser-Emulsionsanlage, Landesamt für Natur, Umwelt und Verbraucherschutz Nordrhein-Westfalen (LANUV), Recklinghausen, LANUV-Fachbericht 77, ISSN 1864-3930 (print), ISSN 2197-7690 (online), 2017.
- Busch, D., Brandt, A., Kleinebrahm, M., and Dreger, S.: Emissionsmessungen auf dem Laborschiff „Max Prüss,“ nach Ausrüstung mit einem SCRT-System: Ein Beitrag zum Projekt Clean Inland Shipping (CLINSH), Landesamt für Natur Umwelt und Verbraucherschutz Nordrhein-Westfalen (LANUV), Recklinghausen, LANUV-Fachbericht 102, <https://edocs.tib.eu/files/e01fn21/1745705619.pdf> (last access: 10 February 2023), 2020.
- CCNR: Rheinschiffsuntersuchungsordnung (RheinSchUO), [https://www.ccr-zkr.org/files/documents/reglementRV/rv1de\\_012022.pdf](https://www.ccr-zkr.org/files/documents/reglementRV/rv1de_012022.pdf) (last access: 10 February 2023), 2020.
- Celik, S., Drewnick, F., Fachinger, F., Brooks, J., Darbyshire, E., Coe, H., Paris, J.-D., Eger, P. G., Schuladen, J., Tadic, I., Friedrich, N., Dienhart, D., Hottmann, B., Fischer, H., Crowley, J. N., Harder, H., and Borrmann, S.: Influence of vessel characteristics and atmospheric processes on the gas and particle phase of ship emission plumes: in situ measurements in the Mediterranean Sea and around the Arabian Peninsula, *Atmos. Chem. Phys.*, 20, 4713–4734, <https://doi.org/10.5194/acp-20-4713-2020>, 2020.
- Cheng, Y., Wang, S., Zhu, J., Guo, Y., Zhang, R., Liu, Y., Zhang, Y., Yu, Q., Ma, W., and Zhou, B.: Surveillance of SO<sub>2</sub> and NO<sub>2</sub> from ship emissions by MAX-DOAS measurements and the implications regarding fuel sulfur content compliance, *Atmos. Chem. Phys.*, 19, 13611–13626, <https://doi.org/10.5194/acp-19-13611-2019>, 2019.
- De Vlieger, I., Int Panis, L., Joul, H., and Cornelis, E.: Fuel consumption and CO<sub>2</sub>-rates for inland vessels, in: Urban Transport X, edited by: Brebbia, C. A. and Wadhwa, L. C., WIT Press, 637–646, ISBN 1-85312-716-7, 2004.
- Diesch, J.-M., Drewnick, F., Klimach, T., and Borrmann, S.: Investigation of gaseous and particulate emissions from various marine vessel types measured on the banks of the Elbe in Northern Germany, *Atmos. Chem. Phys.*, 13, 3603–3618, <https://doi.org/10.5194/acp-13-3603-2013>, 2013.
- DWD Climate Data Center (CDC): Selected 81 stations, distributed over Germany, in the traditional KL-standard format, DWD CDC [data set], [https://opendata.dwd.de/climate\\_environment/CDC/observations\\_germany/climate/subdaily/standard\\_format/DESCRIPTION\\_obsgermany\\_climate\\_subdaily\\_standard\\_format\\_en.pdf](https://opendata.dwd.de/climate_environment/CDC/observations_germany/climate/subdaily/standard_format/DESCRIPTION_obsgermany_climate_subdaily_standard_format_en.pdf), last access: 20 January 2022.
- DWD Climate Data Center (CDC): Historical 10-minute station observations of solar incoming radiation, long-wave downward radiation and sunshine duration for Germany, Version V1, DWD CDC [data set], [https://opendata.dwd.de/climate\\_environment/CDC/observations\\_germany/climate/10\\_minutes/solar/historical/DESCRIPTION\\_obsgermany\\_climate\\_10min\\_solar\\_historical\\_en.pdf](https://opendata.dwd.de/climate_environment/CDC/observations_germany/climate/10_minutes/solar/historical/DESCRIPTION_obsgermany_climate_10min_solar_historical_en.pdf), (last access: 20 January 2022), 2021.
- European Conference of Ministers of Transport: RESOLUTION No. 92/2 ON NEW CLASSIFICATION OF INLAND WATERWAYS, <https://www.itf-oecd.org/sites/default/files/docs/wat19922e.pdf> (last access: 22 March 2023), 1992.
- Eyring, V., Köhler, H. W., van Aardenne, J., and Lauer, A.: Emissions from international shipping: 1. The last 50 years, *J. Geophys. Res.*, 110, D17305, <https://doi.org/10.1029/2004JD005619>, 2005.
- Friedhoff, B., List, S., Hoyer, K., and Tenzer, M.: Bestimmung des effektiven Propellerzustroms, Bundesministerium für Verkehr und digitale Infrastruktur, [https://www.bmvi.de/SharedDocs/DE/Anlage/G/bestimmung-effektiver-propellerzustrom.pdf?\\_\\_blob=publicationFile](https://www.bmvi.de/SharedDocs/DE/Anlage/G/bestimmung-effektiver-propellerzustrom.pdf?__blob=publicationFile) (last access: 22 March 2023), 2018.
- Jiang, H., Di Peng, Wang, Y., and Fu, M.: Comparison of Inland Ship Emission Results from a Real-World Test and an AIS-Based Model, *Atmosphere*, 12, 1611, <https://doi.org/10.3390/atmos12121611>, 2021.
- Kattner, L.: Measurements of shipping emissions with in-situ instruments, PhD thesis, Universität Bremen, <https://doi.org/10.26092/elib/55>, 2019.

- Kattner, L., Mathieu-Üffing, B., Burrows, J. P., Richter, A., Schmolke, S., Seyler, A., and Wittrock, F.: Monitoring compliance with sulfur content regulations of shipping fuel by in situ measurements of ship emissions, *Atmos. Chem. Phys.*, 15, 10087–10092, <https://doi.org/10.5194/acp-15-10087-2015>, 2015.
- Kesgin, U. and Vardar, N.: A study on exhaust gas emissions from ships in Turkish Straits, *Atmos. Environ.*, 35, 1863–1870, [https://doi.org/10.1016/S1352-2310\(00\)00487-8](https://doi.org/10.1016/S1352-2310(00)00487-8), 2001.
- Kleinebrahm, M. and Bourbon, G.-J.: Minderung der Feinstaub-, Ruß- und Stickstoffoxidemissionen auf dem Fahrgastschiff „Jan von Werth“ durch Nachrüstung eines SCRT-Systems, LANUV, Recklinghausen, LANUV-Fachbericht 49, [https://www.lanuv.nrw.de/fileadmin/lanuvpubl/3\\_fachberichte/30049.pdf](https://www.lanuv.nrw.de/fileadmin/lanuvpubl/3_fachberichte/30049.pdf) (last access: 22 March 2023), 2013.
- Klimont, Z., Cofala, J., Bertok, I., Amann, M., Heyes, C., and Gyarfas, F.: Modeling Particulate Emissions in Europe. A Framework to Estimate Reduction Potential and Control Costs, IIASA, Laxenburg, Austria, Interim Report IR-02-076, <https://pure.iiasa.ac.at/id/eprint/6712/> (last access: 22 March 2023), 2002.
- Knörr, W., Heidt, C., Schmied, M., and Notter, B.: Aktualisierung der Emissionsberechnung für die Binnenschifffahrt und Übertragung der Daten in TREMOD, Umweltbundesamt, Dessau-Roßlau, 2013.
- Krause, K., Wittrock, F., Richter, A., Schmitt, S., Pöhler, D., Weigelt, A., and Burrows, J. P.: Estimation of ship emission rates at a major shipping lane by long-path DOAS measurements, *Atmos. Meas. Tech.*, 14, 5791–5807, <https://doi.org/10.5194/amt-14-5791-2021>, 2021.
- Kurtenbach, R., Vaupel, K., Kleffmann, J., Klenk, U., Schmidt, E., and Wiesen, P.: Emissions of NO, NO<sub>2</sub> and PM from inland shipping, *Atmos. Chem. Phys.*, 16, 14285–14295, <https://doi.org/10.5194/acp-16-14285-2016>, 2016.
- Moldanová, J., Fridell, E., Popovicheva, O., Demirdjian, B., Tishkova, V., Faccinotto, A., and Focsa, C.: Characterisation of particulate matter and gaseous emissions from a large ship diesel engine, *Atmos. Environ.*, 43, 2632–2641, <https://doi.org/10.1016/j.atmosenv.2009.02.008>, 2009.
- Pirjola, L., Pajunoja, A., Walden, J., Jalkanen, J.-P., Rönkkö, T., Kousa, A., and Koskentalo, T.: Mobile measurements of ship emissions in two harbour areas in Finland, *Atmos. Meas. Tech.*, 7, 149–161, <https://doi.org/10.5194/amt-7-149-2014>, 2014.
- Prata, A. J.: Measuring SO<sub>2</sub> ship emissions with an ultraviolet imaging camera, *Atmos. Meas. Tech.*, 7, 1213–1229, <https://doi.org/10.5194/amt-7-1213-2014>, 2014.
- Ramacher, M. O. P., Karl, M., Aulinger, A., Bieser, J., Matthias, V., and Quante, M.: The Impact of Emissions from Ships in Ports on Regional and Urban Scale Air Quality, in: *Air Pollution Modeling and its Application XXV*, edited by: Mensink, C. and Kallos, G., Springer Proceedings in Complexity, Springer International Publishing, Cham, 309–316, [https://doi.org/10.1007/978-3-319-57645-9\\_49](https://doi.org/10.1007/978-3-319-57645-9_49), 2018.
- Ramacher, M. O. P., Matthias, V., Aulinger, A., Quante, M., Bieser, J., and Karl, M.: Contributions of traffic and shipping emissions to city-scale NO<sub>x</sub> and PM<sub>2.5</sub> exposure in Hamburg, *Atmos. Environ.*, 237, 117674, <https://doi.org/10.1016/j.atmosenv.2020.117674>, 2020.
- Rohács, J. and Simongáti, G.: The role of inland waterway navigation in a sustainable transport system, *Transport*, 22, 148–153, <https://doi.org/10.3846/16484142.2007.9638117>, 2007.
- Schweighofer, J. and Blaauw, H.: The Cleanest Ship Project – Final Report, 26 pp., <https://doi.org/10.13140/2.1.4202.8326>, 2009.
- Seyler, A., Wittrock, F., Kattner, L., Mathieu-Üffing, B., Peters, E., Richter, A., Schmolke, S., and Burrows, J. P.: Monitoring shipping emissions in the German Bight using MAX-DOAS measurements, *Atmos. Chem. Phys.*, 17, 10997–11023, <https://doi.org/10.5194/acp-17-10997-2017>, 2017.
- Seyler, A., Meier, A. C., Wittrock, F., Kattner, L., Mathieu-Üffing, B., Peters, E., Richter, A., Ruhtz, T., Schönhardt, A., Schmolke, S., and Burrows, J. P.: Studies of the horizontal inhomogeneities in NO<sub>2</sub> concentrations above a shipping lane using ground-based multi-axis differential optical absorption spectroscopy (MAX-DOAS) measurements and validation with airborne imaging DOAS measurements, *Atmos. Meas. Tech.*, 12, 5959–5977, <https://doi.org/10.5194/amt-12-5959-2019>, 2019.
- Tang, L., Ramacher, M. O. P., Moldanová, J., Matthias, V., Karl, M., Johansson, L., Jalkanen, J.-P., Yaramenka, K., Aulinger, A., and Gustafsson, M.: The impact of ship emissions on air quality and human health in the Gothenburg area – Part 1: 2012 emissions, *Atmos. Chem. Phys.*, 20, 7509–7530, <https://doi.org/10.5194/acp-20-7509-2020>, 2020.
- The European Parliament and the European Council: DIRECTIVE 97/68/EC OF THE EUROPEAN PARLIAMENT AND OF THE COUNCIL of 16 December 1997 on the approximation of the laws of the Member States relating to measures against the emission of gaseous and particulate pollutants from internal combustion engines to be installed in non-road mobile machinery, OJ, L 059, 86 pp., <https://eur-lex.europa.eu/legal-content/EN/TXT/PDF/?uri=CELEX:01997L0068-20161006&from=EN> (last access: 22 March 2023), 1998.
- The European Parliament and the European Council: REGULATION (EU) 2016/1628 OF THE EUROPEAN PARLIAMENT AND OF THE COUNCIL of 14 September 2016 on requirements relating to gaseous and particulate pollutant emission limits and type-approval for internal combustion engines for non-road mobile machinery, amending Regulations (EU) No 1024/2012 and (EU) No 167/2013, and amending and repealing Directive 97/68/EC, OJ, L 252, p. 53, <https://eur-lex.europa.eu/legal-content/EN/TXT/?uri=CELEX:02016R1628-20210630> (last access: 22 March 2023), 2016.
- Trozzi, C. and Vaccaro, R.: Methodologies for estimating air pollutant emissions from ships, Technical Report MEET (Methodologies for Estimating Air Pollutant Emissions from Transport) RF98, European Communities, 1998.
- van der Gon, H. D. and Hulskotte, J.: Methodologies for estimating shipping emissions in the Netherlands, A documentation of currently used emission factors and related activity data, BOP report no. 155, Netherlands Environmental Assessment Agency, 56 pp., ISSN: 1875-2322 (print), ISSN: 1875-2314 (online), [https://www.tno.nl/media/2151/methodologies\\_for\\_estimating\\_shipping\\_emissions\\_netherlands.pdf](https://www.tno.nl/media/2151/methodologies_for_estimating_shipping_emissions_netherlands.pdf) (last access: 22 March 2023), 2010.
- van Mensch, P., Abma, D., Verbeek, R., and Hekman, W.: PROMINENT Report D5.7 Technical evaluation of procedures for Certification, Monitoring and Enforcement. Technical evaluation of

- the monitoring results on Rhine, Danube and other vessels, Public report version 2, European Commission, 82 pp., 2018.
- Walden, J., Pirjola, L., Laurila, T., Hatakka, J., Pettersson, H., Walden, T., Jalkanen, J.-P., Nordlund, H., Truuts, T., Meretoja, M., and Kahma, K. K.: Measurement report: Characterization of uncertainties in fluxes and fuel sulfur content from ship emissions in the Baltic Sea, *Atmos. Chem. Phys.*, 21, 18175–18194, <https://doi.org/10.5194/acp-21-18175-2021>, 2021.
- Wang, X., Yi, W., Lv, Z., Deng, F., Zheng, S., Xu, H., Zhao, J., Liu, H., and He, K.: Ship emissions around China under gradually promoted control policies from 2016 to 2019, *Atmos. Chem. Phys.*, 21, 13835–13853, <https://doi.org/10.5194/acp-21-13835-2021>, 2021.
- Zenger, A.: *Atmosphärische Ausbreitungsmodellierung: Grundlagen und Praxis*, Springer, Berlin and Heidelberg, <https://doi.org/10.1007/978-3-642-58979-9>, 1998.
- Zhou, F., Pan, S., Chen, W., Ni, X., and An, B.: Monitoring of compliance with fuel sulfur content regulations through unmanned aerial vehicle (UAV) measurements of ship emissions, *Atmos. Meas. Tech.*, 12, 6113–6124, <https://doi.org/10.5194/amt-12-6113-2019>, 2019.
- Zhou, F., Hou, L., Zhong, R., Chen, W., Ni, X., Pan, S., Zhao, M., and An, B.: Monitoring the compliance of sailing ships with fuel sulfur content regulations using unmanned aerial vehicle (UAV) measurements of ship emissions in open water, *Atmos. Meas. Tech.*, 13, 4899–4909, <https://doi.org/10.5194/amt-13-4899-2020>, 2020.